Nature Communications
https://doi.org/10.1038/s41467-026-76092-4
Article in Press

Spatio-temporal patterns and environmental controls of soil organic carbon stocks in global tidal wetlands since 2009

Received: 27 June 2025
Accepted: 20 July 2026
Published online: 28 July 2026
Cite this article as: Yang, C., Yang, L., Wang, J. *et al.* Spatio-temporal patterns and environmental controls of soil organic carbon stocks in global tidal wetlands since 2009. *Nat Commun* (2026). https://doi.org/10.1038/s41467-026-76092-4

Chenconghai Yang, Lin Yang, Jie Wang, Xiang Li, Lei Zhang & Wenkai Cui

Spatio-temporal patterns and environmental controls of soil organic carbon stocks in global tidal wetlands since 2009

Chenconghai Yang[1], Lin Yang[2*], Jie Wang[1], Xiang Li[1], Lei Zhang[3], Wenkai Cui[1]

[1] School of Geography and Ocean Science, Nanjing University, Nanjing 210023, China

[2] School of Public Administration and Policy, Renmin University of China, Beijing 100872, China

[3] Climate and Ecosystem Sciences Division, Lawrence Berkeley National Laboratory, Berkeley, CA 94720, USA

**Correspondence to*: Lin Yang (yanglin@nju.edu.cn)

Abstract: Tidal wetlands are important blue carbon ecosystems, yet global estimates of soil organic carbon (SOC) stocks and dynamics across mangroves, salt marshes, and tidal flats remain unclear. Using 42,154 records and 63 environmental covariates, we generate global tidal wetland SOC maps for two periods (2009-2014 and 2015-2020) at three depths. Here we show that SOC stocks decrease from $8.80_{2.61}^{20.94}$Pg (mean, 5^{th}-95^{th} percentile prediction interval) to $8.27_{2.27}^{20.61}$Pg, representing a 6.11% decline, with greater losses in deeper layers. Low-latitude regions, particularly South Asia and Africa, are loss hotspots, and lower-middle and upper-middle income countries experience pronounced losses. Mangroves suffer the largest losses primarily due to SOC density decline, whereas salt marshes gain in both area and SOC density. Climate, elevation, and total suspended matter drive mangrove SOC changes; oceanographic factors influence salt marshes and dominate tidal flats. This work reveals the magnitude of blue carbon spatio-temporal change, underscoring the need for targeted conservation.

1 Introduction

Tidal wetlands, which sustain global biodiversity, regulate climatic systems, and enhance human well-being, serve as vital ecosystems for achieving the United Nations Sustainable Development Goals (SDGs) [1,2]. Tidal wetland soil organic carbon (SOC), a critical component of blue carbon systems, has emerged as a global research priority in climate change mitigation due to its substantial carbon storage capacity [3-5]. Compared to most terrestrial ecosystems, tidal wetlands (including mangroves, salt marshes, tidal flats) face far fewer constraints on carbon accumulation [6]. This is primarily attributed to their anaerobic or waterlogged soil conditions, which markedly suppress organic matter decomposition while promoting its accumulation through enhanced deposition [6,7]. Moreover, the prolonged storage of organic carbon in submerged sediments significantly mitigates atmospheric carbon dioxide (CO_2) levels [7]. Facing the urgency of addressing climate change, the role of tidal wetland SOC in the global carbon budget is being increasingly recognized. The Blue Carbon Initiative, launched by Conservation International and the International Union for Conservation of Nature in 2011, advocates for international efforts to protect coastal carbon sinks for climate mitigation [8]. Understanding the spatial distribution, temporal dynamics, and environmental controls of SOC stocks in these ecosystems is therefore essential for developing nature-based solutions for climate mitigation [6,9,10].

Early estimates of SOC stocks in tidal wetlands often relied on averaged values at plot or regional scales [11-15], which overlooked the spatial heterogeneity of carbon distribution [16,17]. Recently, digital soil mapping (DSM) has been widely applied to model the relationships between SOC and environmental covariates and then generate spatially explicit distributions of SOC based on the established relationships [18]. Numerous studies have been conducted regionally, such as in the Great Barrier Reef [19], the tidal wetlands of Australia [13], Amazon [20] or China [21-23], while global assessments are limited to single wetland types, such as global mangroves [24-26] or salt marshes [6]. Tidal flats account for nearly 40% of the global tidal wetland area [27], suggesting a potentially large coastal carbon pool, yet global-scale estimates of tidal flat SOC stocks are scarce [28-30]. The absence of an integrated assessment encompassing mangroves, salt marshes, and tidal flats significantly limits the accuracy of blue carbon accounting and the ability to disentangle their respective contributions.

Tidal wetlands are among the most vulnerable ecosystems [2,31]. Located at the transition zone between land and sea, they are highly sensitive to environmental fluctuations [21], as well as intensified human activities [12,32-36]. Affected by these disturbances, SOC in tidal wetlands is highly dynamic and may undergo substantial changes [32,37,38], even within a decade [36,39-42]. Given their large carbon storage capacity, the potential degradation of tidal wetlands can result in severe carbon emissions, in some cases exceeding those from the loss of equivalent terrestrial ecosystems [5,33]. Thus, research on SOC dynamics in tidal wetlands is receiving increasing attention. Previous assessments of SOC changes in tidal wetlands have largely relied on localized field sampling [35,43,44]. While sampling yields direct and accurate estimates, it is highly costly for large scale applications, and point-based statistical analyses are inadequate for capturing the spatial heterogeneity of carbon dynamics [45-47]. In larger-scale national and global studies, the prevalent method for estimating SOC stock changes relies on tracking tidal wetland area changes while assuming constant SOC density over time [36,48,49]. This approach, however, overlooks the considerable temporal variability in SOC density [50-52]. Besides, global analyses have predominantly focused on mangrove ecosystems [48,49,53,54], leaving other wetland types underrepresented [55]. Recently, spatio-temporal DSM (ST-DSM) has emerged as a cost-effective approach for predicting SOC dynamics, yet its application is largely confined to regional scales [31,56]. Furthermore, the practice of projecting short-term soil-environment relationships over longer timescales raises concerns due to uncertainties in their temporal transferability. It still remains unclear how tidal wetland SOC in all major wetland types has changed globally within a decade. Assessing these major tidal wetland types within a unified and comparable framework enables consistent estimates of total SOC stock changes, allows cross-ecosystem comparisons of controlling factors and processes, and provides a strong foundation for global carbon management and climate mitigation strategies.

Here, we establish spatio-temporal models that predict spatially explicit SOC density in three main tidal wetland types (mangroves, salt marshes, and tidal flats) from 2009 to 2020, and estimate SOC stock changes by explicitly accounting for concurrent variations in both wetland area and SOC density. We delineate the extent of the three tidal wetland categories using a remote sensing derived fine classification system from a global tidal wetland dataset [27]. Soil sample data are collected from multiple existing open-source soil databases, i.e., the Coastal Carbon Research Coordination Network (CCRCN) [57], tidal marsh soil organic carbon (MarSOC) [58], Mangroves soil carbon database [24], World Soil Information Service (WoSIS) [59] and tidal flats samples from coastal China [28] with clearly defined sampling times, comprising 5,489 unique locations (2,245 in mangroves, 2,202 in salt marshes and 1,042 in tidal flats) with 42,154 soil layer records. Additionally, 63 environmental covariates are gathered to characterize oceanography, climate, vegetation, topography, remote sensing, human activities, time and depth factors. Based on the above samples and environmental covariates, separate three-dimensional ST-DSM models are constructed for each wetland type using machine learning. Ultimately, we construct spatially explicit tidal wetland SOC density datasets at three soil depths (0 ~ 30 cm, 30 ~ 60 cm, and 60 ~ 100 cm) at a 90 m spatial resolution for two periods (2009-2014 and 2015-2020), and analyze the SOC stock changes between these two periods from multiple dimensions. Additionally, we quantify the prediction interval ratio (PIR) to evaluate uncertainty and employ interpretable machine learning techniques to identify the main driving factors of tidal wetland SOC dynamics across different tidal wetland types. This study enhances our understanding of the global distribution, dynamics and their driving factors of SOC in tidal wetlands and provides a valuable foundation for wetland conservation and sustainable development.

2 Results

2.1 Global distribution and decadal change hotspots of tidal wetland SOC stocks

We compiled 42,154 soil layer records from 5,489 unique locations, including 16,421 records from 2009-2014 and 25,733 from 2015-2020 (Fig S8). During the 2015-2020 period, global tidal wetlands stored an estimated total SOC of $8.27_{2.27}^{20.61}$ Pg (mean, with a variation range from the 5th to 95th percentile prediction intervals). Tidal wetland SOC stocks exhibited a bell-shaped latitudinal pattern (Fig 1), with 82.1% concentrated between 30°N and 20°S. Relatively high SOC stocks are found in wetlands located in Indonesia in Asia, the low-latitude eastern and western coasts of Africa, and the eastern coast of North America. This pattern is largely related to the widespread presence of mangroves in tropical regions, which have high carbon storage capacity. Spatial patterns of SOC stocks were consistent across soil depths (Fig S1).

The overall SOC stocks within the top 1 m of tidal wetlands declined from $8.80_{2.61}^{20.94}$ Pg (2009-2014) to the aforementioned $8.27_{2.27}^{20.61}$ Pg (2015-2020), resulting in a net loss of 0.53 Pg in the mean, approximately 6.11%. This is equivalent to about 1.98 Pg of additional CO_2 emissions to the atmosphere. The decline in SOC stocks was caused by both the contraction of the tidal wetland area and the reduction in SOC density. Between the two periods, the global tidal wetland area decreased from 348,884.9 km² to 345,934.9 km², with a net loss of 2,950.0 km² (a relative change of 0.85%). At the same time, SOC density (0 ~ 100 cm) fell from $252.33_{74.93}^{600.32}$ Mg/ha to $238.94_{65.64}^{595.72}$ Mg/ha, a decrease of approximately 5.31% (Table 1). The reduction in SOC density contributed more substantially to the total carbon loss than the decrease in wetland area, highlighting the need for greater attention to changes in soil carbon density. We also found that carbon loss intensified with increasing soil depth. While the surface layer (0 ~ 30 cm) exhibited SOC density and SOC stock decreases of 4.59% and 5.40%, respectively, these loss rates in the deep layer (60 ~ 100 cm) rose to 5.90% and 6.69%, respectively (Table 1).

Changes in SOC stocks exhibited substantial spatial heterogeneity (Fig 1), although the spatial distribution patterns remained similar between the two periods (2009-2014 and 2015-2020). SOC stocks declined in most regions, and the equatorial zones, which maintain the largest carbon reservoirs, emerged as particular hotspots of SOC depletion. These equatorial SOC losses are predominantly concentrated in South Asia, the eastern and western coasts of Africa, and the eastern region of South America. Noticeably, areas at 30° N, Northern Europe and the Mozambique

Channel, showed potential for increases in SOC stocks, suggesting these regions could serve as carbon sinks.

Across continents, while Asia held the largest tidal wetland SOC stocks (3.21 Pg in 2015-2020), it also experienced the greatest loss (0.40 Pg). With wetland SOC stocks of 1.20 Pg, Africa also experienced a noticeable carbon decrease (0.09 Pg). SOC stocks in North America (1.89 Pg), South America (0.83 Pg), and Oceania (0.63 Pg) showed slight decreases, while Europe (0.20 Pg) had a slight increase (Fig 1).

Table 1

Fig 1

2.2 Spatio-temporal change of SOC stocks in different tidal wetland types

We collected 13,564 records for mangroves, 24,662 for salt marshes, and 3,928 for tidal flats (Fig S9). Mangroves, with a mean SOC stock of 4.85 Pg, followed by tidal flats with 2.57 Pg and salt marshes with 0.85 Pg, accounted for 58.6%, 31.1%, and 10.2% of the total tidal wetland SOC stocks, respectively (2015-2020, Table 2). Spatially, mangrove SOC stocks were concentrated in equatorial regions, particularly in Indonesia, along the eastern and western coasts of Africa, Mexico, and eastern South America. Salt marshes are largely concentrated around 30°N, corresponding to the strong concentrations along the eastern United States coast. Tidal flats are widely distributed, primarily concentrated in Asia, coasts of North America and parts of Europe (Fig S2).

Across tidal wetland types, mangroves and tidal flats exhibited net average SOC stock declines of 8.41% (0.44 Pg) and 5.67% (0.16 Pg), respectively, whereas salt marshes increased by

7.92% (0.07 Pg, Table 2). Mangrove SOC stock losses were mainly concentrated within 15°S-15°N, declining across most continents, with particularly pronounced losses in Asia and Africa. Tidal flat declines were more broadly distributed within 15°S-30°N, exhibiting widespread continental losses, especially in Asia and South America. In contrast, salt marsh gains were largely concentrated within 20°N-30°N (Fig 2), exhibiting notable increases across several regions, particularly in the Nordic countries, the east coast of China, and the eastern United States. These regional shifts in SOC stocks were caused by distinct combinations of areal and density changes across the three wetland types. For mangroves, the overall stock reduction was primarily driven by a decrease in SOC density (from $324.56_{106.28}^{684.78}$ Mg/ha to $295.85_{85.25}^{668.53}$ Mg/ha), with a relatively stable area (a slight increase from 163,014.61 km² to 163,796.30 km²). Tidal flat SOC stock declines resulted from both area loss (from 141,628.60 km² to 135,816.54 km² with a 4.10% decrease) and reduced SOC density with a relative decrease of 1.64% in the mean. Conversely, in salt marshes, increases in SOC stocks were driven by both increasing SOC density with an increase of 3.07% in the mean, and area expansion (from 44,241.70 km² to 46,322.11 km² with an increase of 4.70%). SOC changes in mangroves and tidal flats were generally consistent across soil layers, whereas salt marsh increases were mainly concentrated in surface and subsurface layers (Fig S3, Table S1).

Table 2

Fig 2

2.3 SOC stock changes in countries at different income levels

Countries at different development stages exhibited distinct patterns of tidal wetland SOC changes. Over the study period, SOC stocks remained relatively stable in high-income countries and the mean SOC stock change in low-income nations showed a slight increase (3.21 Tg). In contrast, substantial losses were observed in most of lower-middle income and upper-middle income countries, with declines of 13.92 Tg and 2.94 Tg on average, respectively (Fig 3A). In the surface layer (0 ~ 30 cm), the difference in carbon change among countries with different income levels was relatively small, whereas in the subsoil (30 ~ 60 cm) and deep soil layers (60 ~ 100 cm), the gap widened, indicating more pronounced disparities in SOC stock dynamics at greater depths (Fig S4).

Among lower-middle income and upper-middle income countries, the most substantial SOC stock losses occurred in Indonesia (-248.5 Tg), followed by Nigeria (-80.1 Tg), Malaysia (-60.3 Tg), Cameroon (-32.6 Tg), Brazil (-29.7 Tg) and Mexico (-23.5 Tg). In contrast, Venezuela exhibited the largest increase (33.5 Tg). The United States, among the high-income countries, recorded the second-highest increase (26.4 Tg). Mozambique and Madagascar, two low-income countries, also showed significant SOC stock growth. Changes in SOC stocks reflected combined shifts in SOC density and wetland area; however, in lower-middle income countries, declines were primarily associated with reductions in SOC density rather than area changes (Fig S4). These results highlight the dominant role of SOC density in shaping overall carbon stock dynamics.

Fig 3

2.4 Key environmental drivers of spatio-temporal SOC in tidal wetlands

Three sets of driver importance results were generated based on SHapley Additive exPlanations (SHAP) values using all the variables, corresponding to mangroves, salt marshes, and tidal flats individually (Fig 4). Covariate importance revealed differences in the key drivers among wetland types, probably related to different SOC change mechanisms (Fig 4A-C). Overall, oceanographic and climatic factors exhibited consistently high importance, highlighting their dominant roles in shaping SOC dynamics across tidal wetlands. Depth-related factors also showed notable importance, especially for salt marshes, highlighting the contribution of vertical soil characteristics.

In mangroves, climatic covariates emerged as particularly important. The minimum annual average temperature was the most important covariate, followed by elevation, total suspended matter (TSM), and precipitation. Notably, population density and gross domestic product (GDP) also exhibited non-negligible influence, indicating the impact of human activities on mangrove ecosystems. The oceanographic factor K2 amplitude was the most important covariate for both salt marshes and tidal flats. In salt marshes, depth-related factors had a large influence, and precipitation, the M2 amplitude, P1 features and minimum temperature also exerted considerable influence. For tidal flats, oceanographic factors played the most important role, followed by the annual average Normalized Difference Vegetation Index (NDVI_Mean), Green band, and precipitation.

Fig 4

3 Discussion

3.1 Advancing the spatio-temporal assessment of global SOC stocks in tidal wetlands

Located at the land-sea interface characterized by intense biogeochemical fluxes and frequent human disturbances, tidal wetlands are among the most vulnerable and dynamic ecosystems on Earth [2,56]. Previous studies have widely demonstrated that the wetland extent can change substantially over decadal timescales, resulting in significant losses in blue carbon stocks [2,36,60]. Moreover, evidence from local, national, and global scales indicates that not only the areal extent but also the SOC density in tidal wetlands can vary considerably within relatively short periods due to environmental changes and anthropogenic disturbances [39,42,61,62], underscoring the need to incorporate SOC temporal variability for more accurate SOC stock assessments. However, the high cost of field data collection has largely restricted previous SOC assessments to regional scales [41,63]. At national and global levels, most estimates of tidal wetland SOC stock changes (summarized in table S3), largely concentrated on mangrove ecosystems, rely predominantly on wetland area changes [26,48,49,53], thereby failing to capture spatial variability in carbon changes and introducing uncertainties into SOC stock dynamics estimates [64].

In this study, we applied a ST-DSM framework to first establish wetland type-specific SOC density-environment relationships from 2009 to 2020 using a comprehensive soil profile dataset, and then to estimate the spatial distribution of SOC stocks for both periods (2009-2014 and 2015-2020) by integrating the predicted SOC density with contemporaneous remote sensing derived wetland extent. In contrast to previous studies that mostly predict changes using short-period soil data (typically collected within a single year [31,56,65]), our study is based on globally distributed samples spanning the entire study period. By integrating these long-term, globally distributed samples with machine learning, our approach effectively captures the evolving soil-environment relationships over the two-decade span. Jointly accounting for changes in wetland area and SOC density yields more accurate spatiotemporal estimations. By applying a standardized covariate pool and modeling architectures to develop ecosystem-specific models, this approach reduces possible methodological inconsistencies and implicit biases when conducting cross-study comparisons [66]. Utilizing a single spatial dataset also resolves boundary ambiguities to prevent the double-counting or omission of transition zones [36]. Crucially, this inclusive framework extends to tidal flats, a massive but historically overlooked coastal carbon pool where sustained sediment deposition drives significant organic matter burial despite lower plant productivity [28,67,68]. By integrating mangroves, salt marshes, and tidal flats into a unified SOC assessment, this study addresses a critical gap in comprehensive blue carbon accounting, provides a more robust and consistent understanding of global coastal wetland soil carbon stocks and dynamics [69], and offers important support for management, conservation planning, and policy decision-making.

3.2 Global tidal wetland SOC stocks compared with prior studies, depth heterogeneity and differences across income level

A few studies have provided evaluations of tidal wetland SOC stocks at the global scale, though primarily focused on individual ecosystems. For mangroves, global SOC stocks are estimated to be 6.4 Pg by Sanderman, et al. [24] with 1,470 records, and 5.00 Pg by Jardine and Siikamäki [25] with 932 records. Recently, Maxwell, et al. [26] reported a lower value of 4.6 Pg in 2020 based on 10,331 records collected over the past sixty years. Our estimate of 4.85 Pg in 2015-2020 is closer to that of Maxwell, et al. [26], possibly due to the similarly large sample size and better representation of mid-latitude mangrove regions in our dataset (Fig S9A, Fig S9D). Alternatively, it is also possible that global mangrove SOC stocks have indeed declined over the past decade, while the studies based on earlier data could not reflect those recent changes [24,25]. Regarding salt marshes, the estimated SOC stocks in this study (0.85 Pg in 2015-2020) are slightly lower than those reported by Maxwell, et al. [6] (1.44 Pg). One possible reason is differences in the definition and classification of salt marsh extent. Our study defines salt marshes with a mapped extent of 46,322.11 km^2 in 2020 based on Zhang, et al. [27]. Yet, the area (52,880 km^2) reported by Maxwell, et al. [6] includes a substantial portion of freshwater system marsh in tidal wetlands [70], which are not considered in our analysis. In terms of SOC density, our estimates are lower than the results of Maxwell, et al. [6] for both surface and deeper soil layers (63.5 Mg/ha vs. 83.1 Mg/ha in 0 ~ 30 cm; 119.0 Mg/ha vs. 185.3 Mg/ha in 0 ~ 100 cm, Table S1). This discrepancy likely reflects differences in SOC accumulation processes, since freshwater marshes typically have higher C: N ratios and more recalcitrant plant material, favoring greater soil organic carbon storage [71,72]. In contrast to the widely investigated mangroves and salt marshes, this study provides a spatially explicit global estimate of SOC stocks in tidal flats, which, to our knowledge, has been lacking in previous research. Earlier studies have estimated their SOC stocks at national or regional scales [28,73,74]. Although tidal flats had the fewest samples among the three wetland types, a sufficient number (3928 records and 1042 profiles) was collected to support robust global modeling (Fig S9C, Fig S9F), achieving an overall Lin's concordance correlation coefficient (LCCC) of 0.74 (Fig S10). Owing to their much broader spatial extent [28], the total SOC stocks in tidal flats exceed half of those in mangroves and are nearly 3 times higher than those in salt marshes, underscoring their substantial contribution to the global blue carbon pool [55].

SOC stock declines are more pronounced in the deeper soil layers than in the surface soils.

This may challenge the conventional view that subsoil organic carbon is relatively less responsive due to inherent physical and chemical protection mechanisms and mineral associations [75]. However, recent evidence suggests that subsoil SOC can be as sensitive to environmental changes as surface SOC in terrestrial ecosystems [76,77]. Our results indicate that deep soil carbon may exhibit considerable variability in a highly dynamic environment. Possible reasons are greater losses of unprotected particulate organic matter in subsoils, limited plant-derived carbon inputs, and accelerated decomposition of aromatic compounds and fatty acids at depth [77,78]. Moreover, previous studies have suggested that the temperature sensitivity of SOC tends to increase with soil depth [79,80], likely due to stronger thermal responses of older and more recalcitrant carbon compounds in the deep layer compared with younger, more labile fractions in the surface layer. This result highlights the critical need to integrate soil depth into SOC modelling and mapping [81,82]. Experimental efforts that examine the depth-dependent responses of wetland SOC to environmental change should be integrated to uncover the underlying mechanisms.

Lower-middle-income and upper-middle-income countries, Indonesia, Nigeria, Malaysia and Cameroon in particular, have experienced greater losses in SOC stocks. In contrast, the average SOC stock changes in high-income or low-income countries have shown stability or a slight increase. This pattern suggests a “U-shaped” relationship between income level and SOC stock changes. High-income countries at a relatively mature stage of development often possess more robust environmental management systems, higher levels of marine funding, and advanced scientific and technological capacities for the conservation and restoration of tidal wetland ecosystems, all of which can contribute to the maintenance and recovery of SOC stocks [10]. Low-income countries, such as Mozambique, Madagascar, and the Gambia, have also shown modest increases in mangrove SOC stocks in recent years [83,84], likely because of limited development capacity and the fact that most economically accessible wetlands have already been converted to shrimp ponds [83,85]. With less anthropogenic interference, the natural regeneration of tidal wetlands may further promote the recovery of their SOC stocks [86]. Lower-middle-income and upper-middle-income countries in Southeast Asia are a global hotspot for SOC stock loss [85]. This may be because these regions are still undergoing intensive development, wetland area loss from land-use conversion, such as the continued transformation of mangroves into oil palm plantations and shrimp farms [32,33,87], as well as reduced SOC density caused by declining mangrove cover, soil exposure, and decreased sedimentation [56,88]. Overall, these findings indicate that a country's stage of socioeconomic development can exert a substantial influence on the direction and magnitude of wetland SOC stock changes.

3.3 Spatial distribution and changes of SOC stocks across three tidal wetland types

Our global assessment reveals spatial and vertical distribution differences among the three wetland types, largely related to their vegetation types. While mangroves hold the largest total SOC stocks and the highest average SOC density, their spatial footprint is restricted to tropical latitudes due to the thermal limits of their woody vegetation [89,90]. Conversely, herbaceous salt marshes mostly grow in temperate or boreal climates. Their SOC is primarily concentrated along the eastern United States coast (Fig S2), where the region's broad, low-gradient coastal plains support a vast and continuous habitat extent [91,92]. Tidal flats, however, being largely unvegetated and unconstrained by plant climatic niches, are widely distributed with primary concentrations in Asia, coasts of North America, and parts of Europe. Beyond these horizontal distribution patterns, our analysis elucidates greater vertical variations in salt marshes, compared to the limited vertical changes observed in mangroves and tidal flats. Previous regional comparisons have yielded contradictory findings regarding whether SOC density in salt marshes or tidal flats is higher. For instance, some localized studies in China suggest that salt marshes hold higher SOC densities due to their relatively abundant vegetation than tidal flats [29,93], whereas others indicate that tidal flats may exhibit higher SOC density in deeper layers [94]. Based on our unified framework, although tidal flats maintain a higher average SOC density overall, salt marshes exhibit higher SOC at the surface, whereas tidal flats are higher in deeper layers (Table S1). Such a phenomenon likely reflects contrasting carbon accumulation mechanisms across depths between the two systems. In salt marshes, SOC typically diminishes with depth as root-derived inputs decrease and aerobic decomposition persists in subsurface layers [94]. Conversely, tidal flats exhibit more vertically consistent SOC profiles.

The changes in SOC stocks differ significantly across the three wetland types. For mangroves, while previous area-based studies estimated a modest ~2% global SOC losses [42,43], our study reveals a much more pronounced 8.41% decline. This trend is particularly evident in Asia (notably Indonesia), which is consistent with the severe mangrove SOC losses reported by Sanderman, et al. [24]. The SOC density decline is widely supported by localized observations across Southeast Asia [42,60] and northern Australia [95]. Tidal flats also exhibited declines in both spatial extent and SOC density, concentrated primarily in tropical regions where land reclamation exerts profound pressures [55,96]. In contrast to mangroves and tidal flats, salt marshes exhibited a net increase in SOC stocks. Both the SOC density and the spatial extent of salt marshes have increased. In salt marshes, Campbell, et al. [36] reported a net loss of 1,452.84 km^2 in salt marsh area since 2000 [36]. However, some recovery after 2009 was also observed, possibly linked to conservation actions such as the U.S. Coastal Master Plan launched in 2009 in Louisiana [36,97], and large-scale salt marsh restoration schemes implemented in China [9,98]. These plans might promote marsh creation and shoreline restoration [36,97], which ultimately fosters the observed increase in SOC density, similar to the findings of a national study [64]. Moreover, we also noticed that changes in SOC stocks of tidal flats and salt marshes are profoundly influenced by trade-offs between them, as these two ecosystems are often geographically adjacent. For example, the simultaneous expansion of salt marshes and contraction of tidal flats was found in regions such as China, the Bay of Bengal and the eastern coast of South America, where significant declines in tidal flat area coincide with increases in salt marsh extent (Fig S7) [99]. This suggests that the rise in salt marsh SOC stocks may come at the cost of shrinking tidal flats. Assessing SOC stock dynamics in salt marshes and tidal flats in isolation may overlook critical cross-habitat conversions. Therefore, the observed rise in salt marsh carbon stocks should be evaluated alongside the concurrent shrinkage of comparatively higher-density tidal flats to fully understand regional carbon dynamics. These findings reinforce the necessity of adopting holistic, cross-ecosystem frameworks in coastal carbon accounting.

3.4 Different environmental controls on SOC in mangroves, salt marshes, and tidal flats

SOC distribution and temporal change in tidal wetlands result from the combined influence of multiple factors [21], with their relative importance varying among different wetland types. Overall, oceanographic factors emerged as important controls on SOC dynamics across all tidal wetlands, reflecting a fundamental difference from the drivers of soil carbon dynamics in terrestrial ecosystems. In mangroves, high SOC density is primarily driven by massive biomass inputs and reduced decomposition [100-102]. It is strongly influenced by seasonal minimum temperature (Fig 4A), which influences plant productivity and associated carbon inputs [89,90]. Similarly, a DSM study on mangroves also identified the minimum temperature as an important driver of SOC patterns [25]. Elevation ranked as the next most important driver in the importance analysis. The significant negative correlation between elevation and mangrove SOC stocks (Fig S6) may be related to the fact that lower elevations are typically associated with slower water flow, facilitating organic matter deposition, which provides the material foundation for SOC formation [101,103,104]. Furthermore, TSM ranked the fourth in mangrove SOC dynamics. While the physical entrapment of allochthonous sediment is traditionally viewed as a subsidy for carbon burial [101,105], our global-scale analysis reveals a counterintuitive negative correlation between total suspended matter and SOC (Pearson's $r = -0.23$, $p < 0.0001$, Fig S6). This pattern suggests that areas with high sediment loads do not necessarily accumulate large SOC stocks [24], likely by reducing light for primary production and enhancing sediment resuspension [106,107]. Notably, despite the projected impact of sea-level rise on global wetland loss [108], sea-level change exhibited relatively low importance in our model, suggesting that climatic and local geomorphic factors may play a more important role than global sea-level change in shaping SOC dynamics. Furthermore, given the significant positive correlation observed between precipitation and mangrove SOC density (Fig S6), the reduction in

SOC may be partially driven by decline of precipitation [109,110]. Human activity indicators demonstrate moderate effects on mangrove SOC, with GDP in particular exhibiting a notable negative correlation (Fig S6). These factors likely serve as proxies for economic development and land use intensity, which in turn affect wetland area changes and SOC dynamics [32,33]. Given their immense ecological and economic value, mangroves have historically been highly susceptible to human exploitation [15,37,42].

Unlike mangrove SOC, which is substantially affected by climate and sustained by dense vegetation biomass, salt marshes and tidal flats are primarily governed by oceanographic factors. For these systems, carbon dynamics is more strongly linked to tidal-mediated external material fluxes than to internal biomass production [55,111-113]. Our analysis identifies tidal constituents, particularly the amplitudes of K2 (lunisolar semidiurnal constituent), as leading predictors of SOC in these systems. Notably, oceanographic drivers exhibit greater importance for tidal flat SOC, with marine variables occupying three of the top four positions (Fig 4C). Such high importance reflects the critical role of exogenous sediment inputs [55], as marine hydrodynamics govern both lateral carbon fluxes and the physical stability of the seabed. For instance, dynamic exchanges of water currents, including tides and waves, can directly import or export carbon into or out of neighboring habitats, and the tidally induced lateral transport of carbon also affects SOC distribution [21,114]. Conversely, intensified wave activity can generate strong suspension effects and cause a more severe disturbance of surface sediments [115], thereby restricting the accumulation of SOC.

Despite these shared oceanographic drivers, salt marshes and tidal flats are differentially influenced by other environmental factors (Fig 4). As herbaceous ecosystems, salt marshes heavily depend on depth-related covariates, driven by vertical processes like deep root activity and salinity migration that regulate vegetation health and carbon preservation [64,116,117]. These vertical processes generate a highly stratified carbon profile, reinforcing previous observations of profound soil heterogeneity in salt marshes, consistent with Maxwell, et al. [6]. In salt marshes, precipitation is more influential than temperature and exhibits a positive correlation with SOC (Fig S6), indicating that hydrological regimes primarily control organic matter inputs. This is because even slight rainfall reductions can increase salinity, suppress vegetation growth, and consequently decrease SOC accumulation [27,118-121]. In tidal flats, however, the importance of the annual average NDVI ranked unexpectedly high despite sparse vegetation (Fig 4C). We also found a positive correlation with SOC, the strongest among all environmental factors (Fig S6). This may be related to the presence of scattered pioneer plants such as microalgae or mosses that locally enhance SOC accumulation [120,121]. Also, NDVI may act as a proxy for related processes, including detritus accumulation and sedimentary organic matter deposition [21,122]. Similar to salt marshes, precipitation also emerged as an influential positive driver for tidal flat SOC density (Fig S6).

3.5 Limitations and future prospects

The possible uncertainty in tidal wetland extent contributes to uncertainty in our SOC estimates. Although the wetland dataset of Zhang, et al. [27] achieves a relatively high overall accuracy (86.44%), it is still subject to errors arising from the inherent limitations of remote sensing-based classification. Remote sensing based classification of mangroves, salt marshes, and tidal flats is often challenging, especially in cases of gradual transitions between wetland types, intricate mixing of wetlands and open water, and areas with sparse historical baseline data [67]. Another potential source of uncertainty is error in remote sensing based tidal wetland classification, such as the frequent misidentification of marshes as open water [27]. These uncertainties in tidal wetland extent may affect the accuracy of tidal wetland SOC stock estimations. Seagrass meadows are also an important type of tidal wetland, but they were not included in this study due to the lack of relevant data, as no temporal dataset for global underwater wetlands is currently available. This is primarily due to their persistent submersion under water, which limits the ability of remote sensing technologies to accurately detect them [27,123]. Future efforts should focus on improving the accuracy and consistency of tidal wetland mapping, particularly in transition zones and data-scarce regions. Additionally, incorporating seagrass meadows into future SOC stock estimations will help provide a more comprehensive understanding of global tidal carbon dynamics.

Overall, the spatial prediction of tidal wetland SOC stocks demonstrated a reliable and satisfactory level of certainty globally, due to the substantially large number of soil samples employed. Predictive uncertainty remains comparatively low in well-sampled hotspots of SOC dynamics, such as the South Asia, the eastern and western coasts of Africa, and the eastern region of South America, underscoring the robustness and reliability of our core estimations (Fig S5). Nevertheless, sample scarcity in certain regions, particularly along the North Atlantic coasts of eastern North America and western Europe, and high-latitude southern South America, still led to higher prediction interval ratio (PIR) (Fig S5). These high pixel-level uncertainties are related to the number and representativeness of samples [124]. Furthermore, when local conditions fall outside the training data domain, the applicability of derived relationships becomes uncertain [125].

Therefore, estimates for these regions should be applied cautiously. Improving the accuracy of estimates relies on increasing sampling density and representativeness through more open and accessible data sharing [125]. This would not only help mitigate the challenges posed by data scarcity but also foster collaborative efforts across regions, leading to more robust and representative estimates of tidal wetland SOC stocks.

Although our models incorporated a comprehensive suite of dozens of covariates spanning climate, oceanography, vegetation, topography, and remote sensing, the absence of data on other factors may limit our understanding of the underlying mechanisms. First, the current lack of globally consistent, high-resolution datasets for geomorphological classes, such as deltas and lagoons, limits the characterization of specific depositional environments [126]. Second, socioeconomic indicators, including population density and GDP serve as useful proxies, yet they fail to fully capture direct human disturbances. Management practices such as aquaculture expansion and deep soil excavation are the critical drivers of SOC changes [62,127]. Access to global, time-series data on these practices in the future would enable a more comprehensive assessment of their evolving impacts and refine our understanding of long-term SOC dynamics. Finally, developing global datasets that characterize dominant species, functional groups, or vegetation assemblages would provide a valuable factor for future SOC modeling, as different plant communities distinctly influence carbon inputs and outputs [6,128]. Filling these critical knowledge gaps will not only refine SOC estimation but also unlock a more predictive understanding of the coastal carbon cycle.

Ultimately, by quantifying SOC dynamics at a high spatial resolution, this study provides a vital foundation for refining global blue carbon inventories and guiding site-specific coastal conservation efforts. The spatially explicit identification of SOC loss hotspots and areas with strong recovery potential establishes a robust baseline for international frameworks such as the Ramsar Convention. Moving forward, these insights should be leveraged to guide cost-effective restoration and promote the sustainable management of the land use of tidal wetland [13]. Continued investment in targeted restoration programs, coupled with enhanced environmental governance and international collaboration, will be instrumental in mitigating further SOC losses and realizing the full climate mitigation potential of tidal blue carbon ecosystems [66].

4 Methods

4.1 Tidal wetland extent data

Due to the scarcity of soil samples and the limited distribution of wetlands in high-latitude regions, the study area was restricted to between 60° N and 60° S [6,70]. We used the tidal wetland types (including mangroves, salt marshes and tidal flats) from the global 30 m wetland dataset with a fine classification system (GWL_FCS30) dataset to define the extent of tidal wetlands [27]. The GWL_FCS30 features a finely detailed land cover classification system and provides annual estimates. Therefore, it can effectively capture the temporal dynamics of the tidal wetland extent across different years [27]. The classification accuracy of the dataset is 86.44%, with a Kappa coefficient of 0.822, and its original spatial resolution is 30 m. In this dataset, mangroves are defined as the forests or shrubs that grow in the coastal brackish or saline water, salt marshes are defined as herbaceous vegetation (grasses, herbs and low shrubs) in the upper coastal intertidal zone, and tidal flats are defined as the tidally flooded zones between the coastal high and low tide levels, including mudflats and sandflats. These definitions were adopted directly from the dataset, and we used the corresponding coastal wetland classes to define the extent of tidal wetlands in this study. Since most key environmental covariates have relatively coarse spatial resolutions, using a finer resolution would not effectively capture environmental differences. Therefore, we chose to resample the dataset to 90 m by the nearest neighbor method [21]. Additionally, a connectivity analysis was performed to remove isolated tidal wetland patches with no adjacent pixels (i.e., wetland patches smaller than two contiguous pixels were excluded) [38,68]. The above operations are unlikely to overestimate or underestimate the wetland area, and thus did not introduce substantial errors in the area or SOC stock estimations. Wetland extents in 2014 and 2020 of GWL_FCS30 served as the prediction extents for 2009-2014 and 2015-2020, respectively. Fig S7 shows the aggregated per 0.5° cell results of the global distribution of mangroves, salt marshes and tidal flats in 2014, 2020, and their changes.

4.2 Soil observation data

The wetland soil samples were integrated from multiple open-source databases, including Coastal Carbon Research Coordination Network (CCRCN) [57], tidal marsh soil organic carbon (MarSOC) [58], Mangroves soil carbon database [24], the World Soil Information Service (WoSIS) [59] and tidal flats sample from coastal China [28]. The soil samples were processed according to the following rules to ensure data quality and consistency. Only samples with clear soil layer depth records (starting depth and ending depth), explicit time labels, and precise geolocation coordinates were retained, with records rounded to only two decimal places excluded. Quality control measures were applied by removing samples with a total soil layer depth of less than 5 cm and those where the upper layer depth exceeded the lower layer depth. Additionally, all records with soil organic carbon (SOC, g/kg) or bulk density (BD, g/cm^3) values of zero were excluded. Samples with starting depths greater than 100 cm were also removed, as they exceeded the scope of the study. We have standardized the units of each dataset. Different databases may contain duplicate records of the same soil layer. For such cases, records with identical values for the year, longitude, latitude, starting depth, ending depth, and SOC were treated as duplicate samples. Additionally, there may be instances where the same soil layer record is reported with differing SOC values (i.e., all fields except SOC are identical). For such cases, we examined the differences between the reported SOC values. If the relative difference was within 30% or the absolute difference was within 20 Mg/ha, the average value was taken. Otherwise, the record was deemed potentially unreliable and excluded from the dataset.

For the CCRCN soil samples that only provided soil organic matter (SOM) data, a new conversion factor of $2.14_{2.15}^{2.13}$ was obtained by fitting a linear regression with a forced intercept of zero (R^2 = 0.96), using paired SOM and SOC records from the soil layers. This new factor replaces the commonly used conversion factor of 1.724 [53]. This modification follows the recommendations of the CCRCN [53,57]. Overall, 41.9% of the total soil layer records in the final dataset used this conversion factor. To include more samples in the training process, soil samples were filtered using the union of the wetland extents from 2009 to 2020. That is, any samples falling within the wetland extent of any given year during this period were considered wetland points and included in the training set.

Finally, we collected a total of 5,489 unique locations and 42,154 soil layer records, including

13,564 mangrove records (2,245 locations), 24,662 salt marsh records (2,202 locations) and 3,928 tidal flat records (1,042 locations), and there were 16,421 records from 2009-2014 and 25,733 records from 2015-2020 (Fig S8). Fig S9 shows the spatial distribution of the soil samples in mangroves, salt marshes and tidal flats. We calculated the environmental representativeness of the collected sample data for each period using six basic environmental covariates (including TSM, M2 amplitude, slope, mean maximum/minimum temperature and precipitation) following the method of Patoine, et al. [129]. The results indicated that 73.52% and 60.44% of the global prediction area for 2009-2014 and 2015-2020, respectively, had chi-square values below 0.975, demonstrating the good representativeness of the samples for global wetland environments.

To address the missing BD data, which account for approximately 8% of the soil layer records that only have SOC measurements, we employed a general machine learning-based pedo-transfer function for imputation [130]. Specifically, we constructed a random forest model for all wetland types using SOC and other key environmental covariates (e.g., depth_min, depth_mid and depth_max, M2 amplitude and M2 phase) to predict BD values (R^2 = 0.92), and it was subsequently used to fill the missing BD values. Because the SOC density showed a left-skewed distribution and digital soil mapping (DSM) models often underestimate extreme values, we log-transformed the target variable using log(x+1) during model fitting, and then back-transformed the outputs to the original scale for prediction [45].

4.3 Static and dynamic environmental covariates

In spatio-temporal digital soil mapping (ST-DSM) modeling, both static and dynamic covariates are used together to build the SOC-environment relationships over time. We adopted seven major categories of environmental covariates to represent the environmental factors, including oceanography, climate, vegetation, topography, remote sensing, and human. In this study, static covariates include the oceanography and topography, dynamic covariates include the sea level change and total suspended matter in oceanography, climate, vegetation, remote sensing and human activities. Oceanographic factors strongly influence SOC through water exchange, carbon transport and sediment deposition [21,114]. Climate, particularly precipitation, regulates hydrology, vegetation productivity and organic matter input [118,119]. Topography and suspended matter affect organic matter retention [103]. Table S2 provides the detailed descriptions. All environmental covariate data are publicly available.

Oceanographic covariates include the amplitudes and phases of the M2, K2 and P1 tidal constituents derived from the FES2014 tidal model (Aviso+) with a 7 km spatial resolution (including amplitude and phase, data resource: https://datastore.cls.fr/catalogues/fes2014-tide-model/) [6,24,131], sea level change from Copernicus with a 0.25 ° spatial resolution (data resource: https://doi.org/10.4

8670/moi-00016) [132], and TSM from MERIS with a 4 km spatial resolution (data resource: https://hermes.acri.fr/) [133]. Climate covariates derived from WorldClim 2.1 (data resource: https://worldclim.org/data/monthlywth.html) [134], include the annual and seasonal averaged maximum temperature (Tmax), minimum temperature (Tmin) and precipitation (Prec). The 4 seasons are defined as March to May, June to August, September to November, and December to February, respectively. Vegetation covariates were derived from the MODIS MOD13Q1 vegetation product and include the maximum, mean, and minimum values of NDVI and EVI, with a 250 m spatial resolution [135]. Remote sensing covariates were derived from Landsat 8 and include both the original spectral bands and various soil moisture, surface salinity, vegetation, surface-brightness and soil texture indices [31,136], with a 30 m spatial resolution. The MOD13Q1 and Landsat 8 data were obtained from Google Earth Engine (GEE, https://earthengine.google.com/), processed to remove clouds and apply scaling factors, and then mean-composited within each of the two study periods to produce a single representative value for each pixel. Topographic covariates include elevation and factors calculated based on elevation layers using SAGA GIS (i.e., Slope, Topographic Wetness Index, Convergence Index, etc.). The topographic base layer was derived from the General Bathymetric Chart of the Oceans (GEBCO), a global digital elevation model (DEM) dataset encompassing both land and ocean surfaces, with an original spatial resolution of approximately 400 m (data resource: https://www.gebco.net/) [137]. Human activity covariates include gross domestic product (GDP) with approximately 900 m spatial resolution (data resource: https://doi.org/10.6084/m9.figshare.17004523.v1) [138], and population from WorldPop with an 800 m spatial resolution (data resource: https://hub.worldpop.org/doi/10.5258/SOTON/WP00647) [139]. All environmental covariates were spatially explicit. Since the study area focuses on tidal wetlands, and some covariates (e.g., climate, TSM, and human activity covariates) were only available over land areas, we used spline interpolation in SAGA GIS to fill in the missing values over the tidal zones [24]. All environmental covariates were harmonized to a spatial resolution of 90 m using the Cubist resampling approach, clipped to the study area, and projected to a unified coordinate reference system (WGS 1984). TSM, vegetation, remote sensing and human activity covariates were further composited into annual mean values.

4.4 Three-dimensional ST-DSM prediction model

We adopted a three-dimensional ST-DSM approach by incorporating soil depth as an explicit predictor covariate during model training [6,140]. By treating depth as a continuous covariate, our method avoids the potential biases of trend-based extrapolation and maximizes the use of all available soil profile data [6,24,140,141]. In addition to using static environmental covariates, we incorporated dynamic environmental covariates corresponding to the specific time period of soil sampling. We also included time covariates, allowing the model to account for temporal changes [56]. SOC density was modeled as a function of depth (d), static environmental covariates (X_s), dynamic environmental covariates (X_d) and time:

$$SOC\ density\ (x, y, t, d) = depth + X_{s1}(x, y) + \cdots + X_{d1}(x, y, t) + \cdots + time \tag{1}$$

where x, y, t, d are 3D+T coordinates of latitude, longitude, time and soil depth; depth includes three covariates: depth_min (starting depth), depth_mid (mean of starting depth and ending depth) and depth_max (ending depth); X_s are the static covariates corresponding to the location (x, y), and X_d are the dynamic covariates corresponding to the location (x, y) and its time period; time is a temporal label in the model, with the sampling year and time period (2009-2014 assigned as 1, and 2015-2020 assigned as 2) of the soil samples.

For modeling, we used samples from each wetland type and constructed three separate models. Dynamic covariates for the two time periods were separately input into the model, producing SOC density predictions for each depth interval (0-30 cm, 30-60 cm, and 60-100 cm) for both periods (2009 -2014 and 2015-2020). After generating the spatial predictions of SOC density, the results were multiplied by the depth factor (3 for 0 ~ 30 cm, 30 ~ 60 cm, and 4 for 60 ~ 100 cm) to obtain the SOC density values in units of Mg/ha [140]. Subsequently, SOC stocks were calculated by multiplying the SOC density by the corresponding area.

The Random Forest (RF) model was chosen for modeling due to its robustness, noise tolerance, and low risk of overfitting [142], making it a popular choice for ST-DSM [143,144]. The RF model was built using the ranger package and performed the Forward Recursive Feature Selection (FRFS) [145-147] to remove redundant covariates and identify the optimal combination of predictors based on the highest Lin's concordance correlation coefficient (LCCC). Afterwards, we tested different combinations of RF parameters (i.e., the number of trees in the forest (ntree) and the number of predictors randomly selected for each tree (mtry)). The environmental covariates and model hyperparameters ultimately selected for each wetland type model are shown in Table S4. Model accuracy, measured by the LCCC, the coefficient of determination (R^2) and the root mean square error (RMSE), was assessed through ten-fold cross-validation. To mitigate spatial dependence between the training and validation sets and prevent accuracy overestimation caused by samples from the same soil profile appearing in both sets, we employed a 10-fold spatial blocking cross validation [6,148]. The number of records in each fold was kept as balanced as possible. Under this stringent validation framework compared to conventional random cross validation [26,149], the overall prediction accuracy achieved an LCCC of 0.65 and an R^2 of 0.46 when combining the three wetlands' samples together (Fig S10). Notably, mangroves, the ecosystem type with the highest SOC density and most pronounced variation, exhibited an LCCC of 0.69 and an R^2 of 0.53 (Fig S10). For comparison, we also performed a conventional random 10-fold cross-validation while preventing profile-based sample leakage, and yielded a higher overall LCCC of 0.77 and R^2 of 0.61 for the three wetlands, and an LCCC of 0.85 and an R^2 of 0.74 for mangroves (Fig S11).

Additionally, the Quantile Random Forest (QRF) model was employed to evaluate predictive uncertainty by extracting the 5th and 95th percentiles (with the "quantreg" parameter set to 0.05 and 0.95) [150]. These values represent the lower and upper bounds of the 90% prediction interval (PI90) [151,152]. The prediction interval ratio (PIR) map was then generated by dividing the PI90 width by the median prediction (50th percentile) [152,153]. To further investigate the importance of individual covariates and explore the driving factors across different wetland types, we applied SHapley Additive exPlanations (SHAP) analysis, a widely used method in interpretable machine learning [154]. SHAP were calculated using the fastshap package, and nsim was set to 100. All covariates, including those excluded by FRFS, were also evaluated in the SHAP analysis, as redundancy in the predictive space does not necessarily preclude causal or ecological relevance, and it also allows us to explore the potential influence of additional environmental factors [155].

Data availability

The wetland extent and environmental covariates used in this study are publicly available. The soil sample data, as well as the prediction results and their upper and lower bounds for SOC stocks at depths of 0 ~ 30 cm, 30 ~ 60 cm, 60 ~ 100 cm, and the integrated 0 ~ 100 cm layer, can be accessed at https://zenodo.org/uploads/19434201.

Code availability

The sample dataset, modeling scripts and trained model in this study have been uploaded to https://zenodo.org/uploads/19434201 (Code upload).

Reference

1 Mumba, M. in *Ramsar Wetlands* (eds Peter A. Gell, Nick C. Davidson, & C. Max Finlayson) xxxi (Elsevier, 2023).

2 Fluet-Chouinard, E. *et al.* Extensive global wetland loss over the past three centuries. *Nature* **614**, 281-286, doi:10.1038/s41586-022-05572-6 (2023).

3 Martinetto, P. *et al.* The blue carbon of southern southwest Atlantic salt marshes and their biotic and abiotic drivers. *Nature Communications* **14**, 8500, doi:10.1038/s41467-023-44196-w (2023).

4 Barbier, E. B. *et al.* The value of estuarine and coastal ecosystem services. *Ecological Monographs* **81**, 169-193, doi:https://doi.org/10.1890/10-1510.1 (2011).

5 Macreadie, P. I. *et al.* Blue carbon as a natural climate solution. *Nature Reviews Earth & Environment* **2**, 826-839, doi:10.1038/s43017-021-00224-1 (2021).

6 Maxwell, T. L. *et al.* Soil carbon in the world's tidal marshes. *Nat. Commun.* **15**, 10265, doi:10.1038/s41467-024-54572-9 (2024).

7 Mcleod, E. *et al.* A blueprint for blue carbon: toward an improved understanding of the role of vegetated coastal habitats in sequestering CO2. *Frontiers in Ecology and the Environment* **9**, 552-560, doi:https://doi.org/10.1890/110004 (2011).

8 Jiao, N., Wang, H., Xu, G. & Aricò, S. Blue carbon on the rise: challenges and opportunities. *Natl. Sci. Rev.* **5**, 464-468, doi:10.1093/nsr/nwy030 (2018).

9 Duarte, C. M., Losada, I. J., Hendriks, I. E., Mazarrasa, I. & Marbà, N. The role of coastal plant communities for climate change mitigation and adaptation. *Nature climate change* **3**, 961-968 (2013).

10 Feng, C. *et al.* Sustainably developing global blue carbon for climate change mitigation and economic benefits through international cooperation. *Nat Commun* **14**, 6144, doi:10.1038/s41467-023-41870-x (2023).

11 Kauffman, J. B., Heider, C., Cole, T. G., Dwire, K. A. & Donato, D. C. Ecosystem Carbon Stocks of Micronesian Mangrove Forests. *Wetlands* **31**, 343-352, doi:10.1007/s13157-011-0148-9 (2011).

12 Fu, C. *et al.* Stocks and losses of soil organic carbon from Chinese vegetated coastal habitats. *Global Change Biology* **27**, 202-214, doi:https://doi.org/10.1111/gcb.15348 (2021).

13 Serrano, O. *et al.* Australian vegetated coastal ecosystems as global hotspots for climate change mitigation. *Nat. Commun.* **10**, 4313, doi:10.1038/s41467-019-12176-8 (2019).

14 Chmura, G. L., Anisfeld, S. C., Cahoon, D. R. & Lynch, J. C. Global carbon sequestration in tidal, saline wetland soils. *Global Biogeochemical Cycles* **17**, doi:https://doi.org/10.1029/2002GB001917 (2003).

15 Atwood, T. B. *et al.* Global patterns in mangrove soil carbon stocks and losses. *Nature Climate Change* **7**, 523-528, doi:10.1038/nclimate3326 (2017).

16 Intergovernmental Panel on Climate Change (IPCC). 2006 IPCC guidelines for national greenhouse gas inventories. *Institute for Global Environmental Strategies, Hayama, Kanagawa, Japan* (2006).

17 Intergovernmental Panel on Climate Change (IPCC). Refinement to the 2006 IPCC guidelines for national greenhouse gas inventories. *IPCC Guidelines for National Greenhouse Gas Inventories.* **3** (2019).

18 McBratney, A. B., Mendonça Santos, M. L. & Minasny, B. On digital soil mapping. *Geoderma* **117**, 3-52, doi:https://doi.org/10.1016/S0016-7061(03)00223-4 (2003).

19 Duarte de Paula Costa, M. *et al.* Current and future carbon stocks in coastal wetlands within the Great Barrier Reef catchments. *Global Change Biology* **27**, 3257-3271,

doi:https://doi.org/10.1111/gcb.15642 (2021).

20 Bernardino, A. F. *et al.* The inclusion of Amazon mangroves in Brazil's REDD+ program. *Nature Communications* **15**, 1549, doi:10.1038/s41467-024-45459-w (2024).

21 Guo, M. *et al.* Hydrology, vegetation, and soil properties as key drivers of soil organic carbon in coastal wetlands: A high-resolution study. *Environ. Sci. Ecotechnol.* **23**, 100482, doi:https://doi.org/10.1016/j.ese.2024.100482 (2025).

22 Meng, W., Feagin, R. A., Hu, B., He, M. & Li, H. The spatial distribution of blue carbon in the coastal wetlands of China. *Estuarine Coastal Shelf Sci.* **222**, 13-20, doi:https://doi.org/10.1016/j.ecss.2019.03.010 (2019).

23 Sun, S. *et al.* A Spatial Baseline of China's Blue Carbon Stocks for Improved Monitoring, Management, and Protection. *Earth's Future* **13**, e2024EF005380, doi:https://doi.org/10.1029/2024EF005380 (2025).

24 Sanderman, J. *et al.* A global map of mangrove forest soil carbon at 30 m spatial resolution. *Environmental Research Letters* **13**, 055002, doi:10.1088/1748-9326/aabe1c (2018).

25 Jardine, S. L. & Siikamäki, J. V. A global predictive model of carbon in mangrove soils. *Environmental Research Letters* **9**, 104013, doi:10.1088/1748-9326/9/10/104013 (2014).

26 Maxwell, T. L. *et al.* Global mangrove soil organic carbon stocks dataset at 30 m resolution for the year 2020 based on spatiotemporal predictive machine learning. *Data Brief* **50**, 109621, doi:https://doi.org/10.1016/j.dib.2023.109621 (2023).

27 Zhang, X. *et al.* GWL_FCS30: a global 30 m wetland map with a fine classification system using multi-sourced and time-series remote sensing imagery in 2020. *Earth Syst. Sci. Data* **15**, 265-293, doi:10.5194/essd-15-265-2023 (2023).

28 Chen, J. *et al.* The Carbon Stock and Sequestration Rate in Tidal Flats From Coastal China. *Global Biogeochem. Cycles* **34**, e2020GB006772, doi:https://doi.org/10.1029/2020GB006772 (2020).

29 Wang, J. *et al.* Unveiling distribution and drivers of soil organic carbon in coastal China: Salt marshes and tidal flats as major carbon storage contributors. *Ecological Indicators* **178**, 114132, doi:https://doi.org/10.1016/j.ecolind.2025.114132 (2025).

30 Wang, F. *et al.* Coastal blue carbon in China as a nature-based solution toward carbon neutrality. *The Innovation* **4**, 100481, doi:https://doi.org/10.1016/j.xinn.2023.100481 (2023).

31 Zhang, S., Tian, J., Lu, X. & Tian, Q. Temporal and spatial dynamics distribution of organic carbon content of surface soil in coastal wetlands of Yancheng, China from 2000 to 2022 based on Landsat images. *CATENA* **223**, 106961, doi:https://doi.org/10.1016/j.catena.2023.106961 (2023).

32 Boone Kauffman, J. *et al.* The jumbo carbon footprint of a shrimp: carbon losses from mangrove deforestation. *Frontiers in Ecology and the Environment* **15**, 183-188, doi:https://doi.org/10.1002/fee.1482 (2017).

33 Kauffman, J. B., Hernandez Trejo, H., del Carmen Jesus Garcia, M., Heider, C. & Contreras, W. M. Carbon stocks of mangroves and losses arising from their conversion to cattle pastures in the Pantanos de Centla, Mexico. *Wetlands Ecology and Management* **24**, 203-216, doi:10.1007/s11273-015-9453-z (2016).

34 Hopkinson, C. S., Cai, W.-J. & Hu, X. Carbon sequestration in wetland dominated coastal systems—a global sink of rapidly diminishing magnitude. *Current Opinion in Environmental Sustainability* **4**, 186-194, doi:https://doi.org/10.1016/j.cosust.2012.03.005 (2012).

35 Kauffman, J. B., Heider, C., Norfolk, J. & Payton, F. Carbon stocks of intact mangroves and carbon emissions arising from their conversion in the Dominican Republic. *Ecological Applications* **24**, 518-

527, doi:https://doi.org/10.1890/13-0640.1 (2014).

36 Campbell, A. D., Fatoyinbo, L., Goldberg, L. & Lagomasino, D. Global hotspots of salt marsh change and carbon emissions. *Nature* **612**, 701-706, doi:10.1038/s41586-022-05355-z (2022).

37 Santos-Andrade, M., Hatje, V., Arias-Ortiz, A., Patire, V. F. & da Silva, L. A. Human disturbance drives loss of soil organic matter and changes its stability and sources in mangroves. *Environ Res* **202**, 111663, doi:10.1016/j.envres.2021.111663 (2021).

38 Hagger, V. *et al.* Drivers of global mangrove loss and gain in social-ecological systems. *Nature Communications* **13**, 6373, doi:10.1038/s41467-022-33962-x (2022).

39 Zhang, C.-y. *et al.* Spatial-temporal characteristics of carbon emissions from land use change in Yellow River Delta region, China. *Ecological Indicators* **136**, 108623, doi:https://doi.org/10.1016/j.ecolind.2022.108623 (2022).

40 Ke, L. *et al.* Estimation of blue carbon stock in the Liaohe Estuary wetland based on soil thickness and multi-scenario modeling. *Ecological Indicators* **171**, 113201, doi:https://doi.org/10.1016/j.ecolind.2025.113201 (2025).

41 Li, Z., Liu, L., Sun, C., Shan, X. & Zhao, H. Spatio-temporal variation and drivers of blue carbon sequestration in Hainan Island, China. *Marine Environmental Research* **197**, 106476, doi:https://doi.org/10.1016/j.marenvres.2024.106476 (2024).

42 Arias-Ortiz, A. *et al.* Losses of Soil Organic Carbon with Deforestation in Mangroves of Madagascar. *Ecosystems* **24**, 1-19, doi:10.1007/s10021-020-00500-z (2021).

43 Tan, L.-S. *et al.* Impacts of land-use change on carbon dynamics in China's coastal wetlands. *Science of The Total Environment* **890**, 164206, doi:https://doi.org/10.1016/j.scitotenv.2023.164206 (2023).

44 Chu, M. *et al.* Temporal variations of mangrove-derived organic carbon storage in two tropical estuaries in Hainan, China since 1960 CE. *Palaeogeography, Palaeoclimatology, Palaeoecology* **627**, 111726, doi:https://doi.org/10.1016/j.palaeo.2023.111726 (2023).

45 Yang, C. *et al.* Spatio-temporal mapping reveals changes in soil organic carbon stocks across the contiguous United States since 1955. *Communications Earth & Environment* **6**, 615, doi:10.1038/s43247-025-02605-6 (2025).

46 Ugbemuna Ugbaje, S. *et al.* Space-time mapping of soil organic carbon stock and its local drivers: Potential for use in carbon accounting. *Geoderma* **441**, 116771, doi:https://doi.org/10.1016/j.geoderma.2023.116771 (2024).

47 Smith, P. *et al.* How to measure, report and verify soil carbon change to realize the potential of soil carbon sequestration for atmospheric greenhouse gas removal. *Global Change Biology* **26**, 219-241, doi:https://doi.org/10.1111/gcb.14815 (2020).

48 Richards, D. R., Thompson, B. S. & Wijedasa, L. Quantifying net loss of global mangrove carbon stocks from 20 years of land cover change. *Nature Communications* **11**, 4260, doi:10.1038/s41467-020-18118-z (2020).

49 Hamilton, S. E. & Friess, D. A. Global carbon stocks and potential emissions due to mangrove deforestation from 2000 to 2012. *Nature Climate Change* **8**, 240-244, doi:10.1038/s41558-018-0090-4 (2018).

50 Nel, L. *et al.* InVEST Soil Carbon Stock Modelling of Agricultural Landscapes as an Ecosystem Service Indicator. *Sustainability* **14** (2022).

51 Luo, K., Samat, A., Van de Voorde, T., Jiang, W. & Abuduwaili, J. Explainable Machine Learning Insights into Wetland Dynamics and Carbon Storage in the Irtysh River Basin. *Earth Systems and Environment*

9, 1793-1820, doi:10.1007/s41748-025-00656-5 (2025).

52 Castillo, J. A. A., Apan, A. A., Maraseni, T. N. & Salmo, S. G. Soil C quantities of mangrove forests, their competing land uses, and their spatial distribution in the coast of Honda Bay, Philippines. *Geoderma* **293**, 82-90, doi:https://doi.org/10.1016/j.geoderma.2017.01.025 (2017).

53 Ouyang, X. & Lee, S. Y. Improved estimates on global carbon stock and carbon pools in tidal wetlands. *Nature Communications* **11**, 317, doi:10.1038/s41467-019-14120-2 (2020).

54 Hengl, T., Maxwell, T. & Parente, L. Predicted soil organic carbon stock at 30 m in t/ha for 0-100 cm depth global / update of the map of mangrove forest soil carbon. *Zenodo*, doi:10.5281/zenodo.7727569 (2018).

55 Chen, Z. L. & Lee, S. Tidal Flats as a Significant Carbon Reservoir in Global Coastal Ecosystems. *Frontiers in Marine Science* **9**, 900896, doi:10.3389/fmars.2022.900896 (2022).

56 Chi, Y., Sun, J., Liu, D. & Xie, Z. Reconstructions of four-dimensional spatiotemporal characteristics of soil organic carbon stock in coastal wetlands during the last decades. *CATENA* **218**, 106553, doi:https://doi.org/10.1016/j.catena.2022.106553 (2022).

57 Coastal Carbon Network. Coastal Carbon Data Library. Smithsonian Environmental Research Center (2025).

58 Maxwell, T. L. *et al.* Global dataset of soil organic carbon in tidal marshes. *Scientific Data* **10**, 797, doi:10.1038/s41597-023-02633-x (2023).

59 Batjes, N. H., Calisto, L. & de Sousa, L. M. Providing quality-assessed and standardised soil data to support global mapping and modelling (WoSIS snapshot 2023). *Earth Syst. Sci. Data* **16**, 4735-4765, doi:10.5194/essd-16-4735-2024 (2024).

60 Richards, D. R. & Friess, D. A. Rates and drivers of mangrove deforestation in Southeast Asia, 2000–2012. *Proceedings of the National Academy of Sciences* **113**, 344-349, doi:doi:10.1073/pnas.1510272113 (2016).

61 Ju, C. *et al.* Global Declines in Mangrove Area and Carbon-Stock From 1985 to 2020. *Geophysical Research Letters* **52**, e2025GL115303, doi:https://doi.org/10.1029/2025GL115303 (2025).

62 Fu, C. *et al.* Nonuniform organic carbon stock loss in soils across disturbed blue carbon ecosystems. *Nature Communications* **16**, 4370, doi:10.1038/s41467-025-59752-9 (2025).

63 Ghosh, R. & Mitra, A. Decadal Variation of Soil Organic Carbon Stock in the Mangrove-Dominated Indian Sundarbans. *Eurasian Soil Science* **58**, 15, doi:10.1134/S1064229324602051 (2025).

64 Fan, B. & Li, Y. China's conservation and restoration of coastal wetlands offset much of the reclamation-induced blue carbon losses. *Global Change Biol.* **30**, e17039, doi:https://doi.org/10.1111/gcb.17039 (2024).

65 Young, M. A. *et al.* National scale predictions of contemporary and future blue carbon storage. *Sci. Total Environ.* **800**, 149573, doi:https://doi.org/10.1016/j.scitotenv.2021.149573 (2021).

66 Macreadie, P. I. *et al.* The future of Blue Carbon science. *Nature Communications* **10**, 3998, doi:10.1038/s41467-019-11693-w (2019).

67 Murray, N. J. *et al.* The global distribution and trajectory of tidal flats. *Nature* **565**, 222-225, doi:10.1038/s41586-018-0805-8 (2019).

68 Murray, N. J. *et al.* High-resolution global maps of tidal flat ecosystems from 1984 to 2019. *Sci Data* **9**, 542, doi:10.1038/s41597-022-01635-5 (2022).

69 Alongi, D. M. Carbon Balance in Salt Marsh and Mangrove Ecosystems: A Global Synthesis. *J. Mar. Sci. Eng.* **8**, 767 (2020).

70 Worthington, T. A. *et al.* The distribution of global tidal marshes from Earth observation data. *Global Ecology and Biogeography* **33**, e13852, doi:https://doi.org/10.1111/geb.13852 (2024).

71 Jones, J. A., Cherry, J. A. & McKee, K. L. Species and tissue type regulate long-term decomposition of brackish marsh plants grown under elevated CO2 conditions. *Estuarine Coastal Shelf Sci.* **169**, 38-45, doi:https://doi.org/10.1016/j.ecss.2015.11.033 (2016).

72 Van de Broek, M., Temmerman, S., Merckx, R. & Govers, G. Controls on soil organic carbon stocks in tidal marshes along an estuarine salinity gradient. *Biogeosciences* **13**, 6611-6624, doi:10.5194/bg-13-6611-2016 (2016).

73 Hinson, A. L. *et al.* The spatial distribution of soil organic carbon in tidal wetland soils of the continental United States. *Global Change Biology* **23**, 5468-5480, doi:https://doi.org/10.1111/gcb.13811 (2017).

74 Wang, M. *et al.* Distribution and Storage Characteristics of Soil Organic Carbon in Tidal Wetland of Dandou Sea, Guangxi. *Atmosphere* **15**, 431 (2024).

75 Harrison, R. B., Footen, P. W. & Strahm, B. D. Deep Soil Horizons: Contribution and Importance to Soil Carbon Pools and in Assessing Whole-Ecosystem Response to Management and Global Change. *Forest Science* **57**, 67-76, doi:10.1093/forestscience/57.1.67 (2011).

76 Hicks Pries, C. E., Castanha, C., Porras, R. C. & Torn, M. S. The whole-soil carbon flux in response to warming. *Science* **355**, 1420-1423, doi:10.1126/science.aal1319 (2017).

77 Soong, J. L. *et al.* Five years of whole-soil warming led to loss of subsoil carbon stocks and increased CO2 efflux. *Science Advances* **7**, eabd1343, doi:10.1126/sciadv.abd1343.

78 Ofiti, N. O. E. *et al.* Warming promotes loss of subsoil carbon through accelerated degradation of plant-derived organic matter. *Soil Biology and Biochemistry* **156**, 108185, doi:https://doi.org/10.1016/j.soilbio.2021.108185 (2021).

79 Hilasvuori, E. *et al.* Temperature sensitivity of decomposition in a peat profile. *Soil Biology and Biochemistry* **67**, 47-54, doi:https://doi.org/10.1016/j.soilbio.2013.08.009 (2013).

80 Li, J. *et al.* Rising Temperature May Trigger Deep Soil Carbon Loss Across Forest Ecosystems. *Advanced Science* **7**, 2001242, doi:https://doi.org/10.1002/advs.202001242 (2020).

81 Luo, Z., Viscarra Rossel, R. A. & Shi, Z. Distinct controls over the temporal dynamics of soil carbon fractions after land use change. *Global Change Biol.* **26**, 4614-4625, doi:https://doi.org/10.1111/gcb.15157 (2020).

82 Liu, C. *et al.* Molecular insight into the vertical migration and degradation of dissolved organic matter in riparian soil profiles. *Environ. Res.* **245**, 118013, doi:https://doi.org/10.1016/j.envres.2023.118013 (2024).

83 Naidoo, G. The mangroves of Africa: A review. *Marine Pollution Bulletin* **190**, 114859, doi:https://doi.org/10.1016/j.marpolbul.2023.114859 (2023).

84 Muthee, K. *et al.* Mangrove ecosystems mapping in parts of Ghana and The Gambia for sustainable regeneration and utilization. *Anthropocene Coasts* **8**, 9, doi:10.1007/s44218-025-00073-1 (2025).

85 Goldberg, L., Lagomasino, D., Thomas, N. & Fatoyinbo, T. Global declines in human-driven mangrove loss. *Global Change Biology* **26**, 5844-5855, doi:https://doi.org/10.1111/gcb.15275 (2020).

86 Thura, K. *et al.* Mangrove restoration built soil organic carbon stocks over six decades: a chronosequence study. *Journal of Soils and Sediments* **23**, 1193-1203, doi:10.1007/s11368-022-03418-2 (2023).

87 Rahman *et al.* Mangrove ecosystems in Southeast Asia region: Mangrove extent, blue carbon potential and CO(2) emissions in 1996-2020. *Sci Total Environ* **915**, 170052, doi:10.1016/j.scitotenv.2024.170052

(2024).

88 Jones, T. G., Ratsimba, H. R., Ravaoarinorotsihoarana, L., Cripps, G. & Bey, A. Ecological Variability and Carbon Stock Estimates of Mangrove Ecosystems in Northwestern Madagascar. *Forests* **5**, 177-205 (2014).

89 Cavanaugh, K. C. *et al.* Poleward expansion of mangroves is a threshold response to decreased frequency of extreme cold events. *Proceedings of the National Academy of Sciences* **111**, 723-727, doi:doi:10.1073/pnas.1315800111 (2014).

90 Cavanaugh, K. C. *et al.* Sensitivity of mangrove range limits to climate variability. *Global Ecology and Biogeography* **27**, 925-935, doi:https://doi.org/10.1111/geb.12751 (2018).

91 Braswell, A. E., Heffernan, J. B. & Kirwan, M. L. How Old Are Marshes on the East Coast, USA? Complex Patterns in Wetland Age Within and Among Regions. *Geophysical Research Letters* **47**, e2020GL089415, doi:https://doi.org/10.1029/2020GL089415 (2020).

92 Turek, B., Teng, W., Yu, Q., Yellen, B. & Woodruff, J. Modeling Spatial Distributions of Salt Marsh Blue Carbon Using Morphometric Parameters From Lidar. *Journal of Geophysical Research: Earth Surface* **130**, e2024JF007676, doi:https://doi.org/10.1029/2024JF007676 (2025).

93 Mao, Y., Ma, Q., Lin, J., Chen, Y. & Shu, Q. Distribution and Sources of Organic Carbon in Surface Intertidal Sediments of the Rudong Coast, Jiangsu Province, China. *Journal of Marine Science and Engineering* **9**, 992 (2021).

94 Yu, B. *et al.* Recalcitrant organic carbon in deep soils plays a greater role in soil carbon sequestration under tidal flat than vegetated salt marsh. *CATENA* **259**, 109412, doi:https://doi.org/10.1016/j.catena.2025.109412 (2025).

95 Sippo, J. Z. *et al.* Coastal carbon cycle changes following mangrove loss. *Limnology and Oceanography* **65**, 2642-2656, doi:https://doi.org/10.1002/lno.11476 (2020).

96 Lee, S. Y. & Khim, J. S. Hard science is essential to restoring soft-sediment intertidal habitats in burgeoning East Asia. *Chemosphere* **168**, 765-776, doi:https://doi.org/10.1016/j.chemosphere.2016.10.136 (2017).

97 Coastal Protection and Restoration Authority of Louisiana. Louisiana comprehensive master plan for a sustainable coast. *Coastal Protection and Restoration Authority of Louisiana* (2012).

98 An, S. *et al.* China's natural wetlands: past problems, current status, and future challenges. *AMBIO: A Journal of the Human Environment* **36**, 335-342 (2007).

99 Jackson, M. V. *et al.* Dual threat of tidal flat loss and invasive Spartina alterniflora endanger important shorebird habitat in coastal mainland China. *Journal of Environmental Management* **278**, 111549, doi:https://doi.org/10.1016/j.jenvman.2020.111549 (2021).

100 Donato, D. C. *et al.* Mangroves among the most carbon-rich forests in the tropics. *Nature Geoscience* **4**, 293-297, doi:10.1038/ngeo1123 (2011).

101 Alongi, D. M. Carbon Cycling and Storage in Mangrove Forests. *Annual Review of Marine Science* **6**, 195-219, doi:https://doi.org/10.1146/annurev-marine-010213-135020 (2014).

102 Sarker, S., Masud-Ul-Alam, M., Hossain, M. S., Rahman Chowdhury, S. & Sharifuzzaman, S. M. A review of bioturbation and sediment organic geochemistry in mangroves. *Geological Journal* **56**, 2439-2450, doi:https://doi.org/10.1002/gj.3808 (2021).

103 Connor, R. F., Chmura, G. L. & Beecher, C. B. Carbon accumulation in bay of fundy salt marshes: Implications for restoration of reclaimed marshes. *Global Biogeochemical Cycles* **15**, 943-954, doi:https://doi.org/10.1029/2000GB001346 (2001).

104 Rogers, K., Macreadie, P. I., Kelleway, J. J. & Saintilan, N. Blue carbon in coastal landscapes: a spatial framework for assessment of stocks and additionality. *Sustainability Science* **14**, 453-467, doi:10.1007/s11625-018-0575-0 (2019).

105 Zhang, J. *et al.* A global assessment of mangrove soil organic carbon sources and implications for blue carbon credit. *Nature Communications* **15**, 8994, doi:10.1038/s41467-024-53413-z (2024).

106 Morgan, K. M., Moynihan, M. A., Sanwlani, N. & Switzer, A. D. Light limitation and depth-variable sedimentation drives vertical reef compression on turbid coral reefs. *Frontiers in Marine Science* **7**, 571256 (2020).

107 Bartl, I. & Thrush, S. Sediment heterogeneity affects variability of resuspension-induced CO2 production. *EGUsphere* **2025**, 1-18, doi:10.5194/egusphere-2025-3045 (2025).

108 Schuerch, M. *et al.* Future response of global coastal wetlands to sea-level rise. *Nature* **561**, 231-234, doi:10.1038/s41586-018-0476-5 (2018).

109 Osland, M. J. *et al.* Climatic controls on the global distribution, abundance, and species richness of mangrove forests. *Ecological Monographs* **87**, 341-359, doi:https://doi.org/10.1002/ecm.1248 (2017).

110 Deng, L. *et al.* Drought effects on soil carbon and nitrogen dynamics in global natural ecosystems. *Earth-Science Reviews* **214**, 103501, doi:https://doi.org/10.1016/j.earscirev.2020.103501 (2021).

111 Li, T. *et al.* The isotopic composition of organic carbon, nitrogen and provenance of organic matter in surface sediment from the Jiangsu tidal flat, southwestern Yellow Sea. *Marine Pollution Bulletin* **182**, 114010, doi:https://doi.org/10.1016/j.marpolbul.2022.114010 (2022).

112 Osland, M. J. *et al.* Climate and plant controls on soil organic matter in coastal wetlands. *Global Change Biol.* **24**, 5361-5379, doi:https://doi.org/10.1111/gcb.14376 (2018).

113 Yando, E. S. *et al.* Salt marsh-mangrove ecotones: using structural gradients to investigate the effects of woody plant encroachment on plant–soil interactions and ecosystem carbon pools. *Journal of Ecology* **104**, 1020-1031, doi:https://doi.org/10.1111/1365-2745.12571 (2016).

114 Bogard, M. J. *et al.* Hydrologic Export Is a Major Component of Coastal Wetland Carbon Budgets. *Global Biogeochemical Cycles* **34**, e2019GB006430, doi:https://doi.org/10.1029/2019GB006430 (2020).

115 Mudd, S. M., D'Alpaos, A. & Morris, J. T. How does vegetation affect sedimentation on tidal marshes? Investigating particle capture and hydrodynamic controls on biologically mediated sedimentation. *Journal of Geophysical Research: Earth Surface* **115**, doi:https://doi.org/10.1029/2009JF001566 (2010).

116 Hinson, A. L., Feagin, R. A. & Eriksson, M. Environmental Controls on the Distribution of Tidal Wetland Soil Organic Carbon in the Continental United States. *Global Biogeochemical Cycles* **33**, 1408-1422, doi:https://doi.org/10.1029/2019GB006179 (2019).

117 Ni, X. *et al.* Source and degradation of soil organic matter in different vegetations along a salinity gradient in the Yellow River Delta wetland. *CATENA* **248**, 108603, doi:https://doi.org/10.1016/j.catena.2024.108603 (2025).

118 Osland, M. J. *et al.* Climate and plant controls on soil organic matter in coastal wetlands. *Glob Chang Biol* **24**, 5361-5379, doi:10.1111/gcb.14376 (2018).

119 Feher, L. C. *et al.* Linear and nonlinear effects of temperature and precipitation on ecosystem properties in tidal saline wetlands. *Ecosphere* **8**, e01956, doi:https://doi.org/10.1002/ecs2.1956 (2017).

120 Corzo, A. *et al.* Intertidal microphytobenthic primary production and net metabolism of a tropical estuary. *Mar Environ Res* **202**, 106741, doi:10.1016/j.marenvres.2024.106741 (2024).

121 Abed, R. M. M. *et al.* Lipid biomarkers, pigments and cyanobacterial diversity of microbial mats across intertidal flats of the arid coast of the Arabian Gulf (Abu Dhabi, UAE). *FEMS Microbiology Ecology* **65**,

449-462, doi:10.1111/j.1574-6941.2008.00537.x (2008).
122 Suir, G. M. & Sasser, C. E. Use of NDVI and Landscape Metrics to Assess Effects of Riverine Inputs on Wetland Productivity and Stability. *Wetlands* **39**, 815-830, doi:10.1007/s13157-019-01132-3 (2019).
123 Richardson, D. C. *et al.* A functional definition to distinguish ponds from lakes and wetlands. *Scientific Reports* **12**, 10472, doi:10.1038/s41598-022-14569-0 (2022).
124 Zhang, L. *et al.* An adaptive uncertainty-guided sampling method for geospatial prediction and its application in digital soil mapping. *International Journal of Geographical Information Science* **37**, 1-23, doi:10.1080/13658816.2022.2125973 (2022).
125 Meyer, H. & Pebesma, E. Predicting into unknown space? Estimating the area of applicability of spatial prediction models. *Methods in Ecology and Evolution* **12**, 1620-1633, doi:https://doi.org/10.1111/2041-210X.13650 (2021).
126 Kirwan, M. L., Megonigal, J. P., Noyce, G. L. & Smith, A. J. Geomorphic and ecological constraints on the coastal carbon sink. *Nature Reviews Earth & Environment* **4**, 393-406, doi:10.1038/s43017-023-00429-6 (2023).
127 Lovelock, C. E. *et al.* Assessing the risk of carbon dioxide emissions from blue carbon ecosystems. *Frontiers in Ecology and the Environment* **15**, 257-265 (2017).
128 Smeaton, C. *et al.* Using citizen science to estimate surficial soil Blue Carbon stocks in Great British saltmarshes. *Frontiers in Marine Science* **9**, 959459 (2022).
129 Patoine, G. *et al.* Drivers and trends of global soil microbial carbon over two decades. *Nat. Commun.* **13**, 4195, doi:10.1038/s41467-022-31833-z (2022).
130 Wang, M. *et al.* Global soil profiles indicate depth-dependent soil carbon losses under a warmer climate. *Nat. Commun.* **13**, 5514, doi:10.1038/s41467-022-33278-w (2022).
131 Lyard, F. H., Allain, D. J., Cancet, M., Carrère, L. & Picot, N. FES2014 global ocean tide atlas: design and performance. *Ocean Sci.* **17**, 615-649, doi:10.5194/os-17-615-2021 (2021).
132 Mercator Ocean International & Copernicus Marine Service. Copernicus Marine Environment Monitoring Service. Copernicus Marine Service (2026).
133 Doerffer, R. & Schiller, H. The MERIS Case 2 water algorithm. *Int. J. Remote Sens.* **28**, 517-535, doi:10.1080/01431160600821127 (2007).
134 Fick, S. E. & Hijmans, R. J. WorldClim 2: new 1-km spatial resolution climate surfaces for global land areas. *Int. J. Climatol.* **37**, 4302-4315, doi:https://doi.org/10.1002/joc.5086 (2017).
135 Didan, K. MOD13Q1 MODIS/Terra vegetation indices 16-day L3 global 250m SIN grid V006. *NASA EOSDIS Land Processes Distributed Active Archive Center (DAAC) data set*, MOD13Q11. 006 (2015).
136 U.S. Geological Survey. Landsat 8 Collection 2 Level-1. U.S. Geological Survey https://doi.org/10.5066/P9/LS8 (2019).
137 Schenke, H. W. in *Encyclopedia of Marine Geosciences* (eds Jan Harff, Martin Meschede, Sven Petersen, & JÖrn Thiede) 268-269 (Springer Netherlands, 2016).
138 Chen, J. *et al.* Global 1 km × 1 km gridded revised real gross domestic product and electricity consumption during 1992–2019 based on calibrated nighttime light data. *Scientific Data* **9**, 202, doi:10.1038/s41597-022-01322-5 (2022).
139 WorldPop & Center for International Earth Science Information Network (CIESIN), Columbia University. WorldPop Global Project Population Data. WorldPop (2018).
140 Hengl, T. & MacMillan, R. A. *Predictive Soil Mapping with R.* (Lulu Press, Incorporated, 2018).
141 Helfenstein, A., Mulder, V. L., Heuvelink, G. B. M. & Hack-ten Broeke, M. J. D. Three-dimensional space

and time mapping reveals soil organic matter decreases across anthropogenic landscapes in the Netherlands. *Commun. Earth Environ.* **5**, 130, doi:10.1038/s43247-024-01293-y (2024).

142 Breiman, L. Random Forests. *Machine Learning* **45**, 5-32, doi:https://doi.org/10.1023/A:1010933404324 (2001).

143 Heuvelink, G. B. M. *et al.* Machine learning in space and time for modelling soil organic carbon change. *Eur. J. Soil Sci.* **72**, 1607-1623, doi:https://doi.org/10.1111/ejss.12998 (2021).

144 Li, N., Zhou, S. & Margenot, A. J. From prairie to crop: Spatiotemporal dynamics of surface soil organic carbon stocks over 167 years in Illinois, U.S.A. *Sci. Total Environ.* **857**, 159038, doi:https://doi.org/10.1016/j.scitotenv.2022.159038 (2023).

145 Liu, Y. *et al.* Improving digital mapping of soil organic matter in cropland by incorporating crop rotation. *Geoderma* **438**, 116620, doi:https://doi.org/10.1016/j.geoderma.2023.116620 (2023).

146 Hu, B. *et al.* Fine-resolution mapping of cropland topsoil pH of Southern China and its environmental application. *Geoderma* **442**, 116798, doi:https://doi.org/10.1016/j.geoderma.2024.116798 (2024).

147 Meyer, H., Reudenbach, C., Wöllauer, S. & Nauss, T. Importance of spatial predictor variable selection in machine learning applications – Moving from data reproduction to spatial prediction. *Ecol. Modell.* **411**, 108815, doi:https://doi.org/10.1016/j.ecolmodel.2019.108815 (2019).

148 Ludwig, M., Moreno-Martinez, A., Hölzel, N., Pebesma, E. & Meyer, H. Assessing and improving the transferability of current global spatial prediction models. *Global Ecol. Biogeogr.* **32**, 356-368, doi:https://doi.org/10.1111/geb.13635 (2023).

149 Gasch, C. K. *et al.* Spatio-temporal interpolation of soil water, temperature, and electrical conductivity in 3D + T: The Cook Agronomy Farm data set. *Spatial Statistics* **14**, 70-90, doi:https://doi.org/10.1016/j.spasta.2015.04.001 (2015).

150 Meinshausen, N. & Ridgeway, G. Quantile Regression Forests. *Journal of Machine Learning Research* **7**, 983-999 (2006).

151 Arrouays, D., Mulder, V. L. & Richer-de-Forges, A. C. Soil mapping, digital soil mapping and soil monitoring over large areas and the dimensions of soil security – A review. *Soil Security* **5**, 100018, doi:https://doi.org/10.1016/j.soisec.2021.100018 (2021).

152 Poggio, L. *et al.* SoilGrids 2.0: producing soil information for the globe with quantified spatial uncertainty. *SOIL* **7**, 217-240, doi:10.5194/soil-7-217-2021 (2021).

153 Zhang, L. *et al.* Mapping global distributions, environmental controls, and uncertainties of apparent topsoil and subsoil organic carbon turnover times. *Earth Syst. Sci. Data* **17**, 2605-2623, doi:10.5194/essd-17-2605-2025 (2025).

154 Štrumbelj, E. & Kononenko, I. Explaining prediction models and individual predictions with feature contributions. *Knowledge and Information Systems* **41**, 647-665, doi:10.1007/s10115-013-0679-x (2014).

155 Wadoux, A. M. J. C., Samuel-Rosa, A., Poggio, L. & Mulder, V. L. A note on knowledge discovery and machine learning in digital soil mapping. *European Journal of Soil Science* **71**, 133-136, doi:https://doi.org/10.1111/ejss.12909 (2020).

Funding Statement

This study is supported by the National Natural Science Foundation of China (Project No. 42471468), the Fundamental Research Funds for the Central Universities, and the Research Funds of Renmin University of China (26XNSJ23).

Author Contributions Statement

C.C.H.Y: Writing - original draft, Writing – review & editing, Visualization, Validation, Supervision, Software, Resources, Project administration, Methodology, Investigation, Formal analysis, Data curation, Conceptualization. **L.Y:** Writing - review & editing, Supervision, Resources, Methodology, Funding acquisition, Conceptualization. **J.W:** Software, Resources, Methodology, **X.L:** Writing - review & editing. **L.Z:** Writing - review & editing, Validation. **W.K.C:** Methodology.

Competing Interests Statement

The authors declare no competing interests.

Tables

Table 1 Global soil organic carbon (SOC) density (Mg/ha) and stocks (Pg) at different soil depths (0 ~ 30 cm, 30 ~ 60 cm, 60 ~ 100 cm and total 0 ~ 100 cm) in 2009-2014 and 2015- 2020, along with their change rates calculated based on mean values.

Depth (cm)	SOC density in 2009-2014 (Mg/ha)	SOC density in 2015-2020 (Mg/ha)	Relative change rate	SOC stocks in 2009-2014 (Pg)	SOC stocks in 2015-2020 (Pg)	Relative change rate
0~30	$77.95_{25.47}^{179.68}$	$74.37_{22.58}^{178.99}$	-4.59%	$2.72_{0.89}^{6.27}$	$2.57_{0.78}^{6.19}$	-5.40%
30~60	$76.31_{22.87}^{180.35}$	$72.28_{22.87}^{178.32}$	-5.28%	$2.66_{0.80}^{6.29}$	$2.50_{0.69}^{6.17}$	-6.08%
60~100	$98.06_{26.59}^{240.29}$	$92.28_{23.06}^{238.41}$	-5.90%	$3.42_{0.93}^{8.38}$	$3.19_{0.80}^{8.25}$	-6.69%
0~100	$252.33_{74.93}^{600.32}$	$238.94_{65.64}^{595.72}$	-5.31%	$8.80_{2.61}^{20.94}$	$8.27_{2.27}^{20.61}$	-6.11%

Table 2 Soil organic carbon (SOC) density (Mg/ha) and SOC stocks (Pg) of mangroves, salt marshes, and tidal flats during 2009-2014 and 2015-2020, and their relative change rates calculated based on mean values (0 ~ 100 cm soil depth).

Wetland type	SOC density in 2009-2014 (Mg/ha)	SOC density in 2015-2020 (Mg/ha)	Relative change rate	SOC stocks in 2009-2014 (Pg)	SOC stocks in 2015-2020 (Pg)	Relative change rate
Mangroves	$324.56_{106.28}^{684.78}$	$295.85_{85.25}^{668.53}$	-8.85%	$5.29_{1.73}^{11.16}$	$4.85_{1.40}^{10.95}$	-8.41%
Salt marshes	$177.07_{47.51}^{499.76}$	$182.51_{51.36}^{521.54}$	3.07%	$0.78_{0.21}^{2.21}$	$0.85_{0.24}^{2.42}$	7.92%
Tidal flats	$192.69_{47.42}^{534.54}$	$189.54_{46.85}^{533.21}$	-1.64%	$2.73_{0.67}^{7.57}$	$2.57_{0.64}^{7.24}$	-5.67%

Figure Legends/Captions

Fig 1 Aggregated per 0.5° cell results of global distribution, latitudinal patterns, and continental bar plots of soil organic carbon (SOC) stocks and their changes of all wetland types from 2009 to 2020 (0 ~ 100 cm soil depth, summarized from wetland type specific models). The bar graph shows the SOC stocks (Pg), SOC density (Mg/ha), and wetland area (10^3 km^2) of each continent and their change. The change curves are calculated based on the mean SOC stock estimates. Note: AF:

Africa; AS: Asia; OA: Australia and Oceania; EU: Europe; NA: North America; SA: South America. The gray shading represents the range of the 5th and 95th percentile prediction intervals. Results for different soil depth intervals are provided in Fig S1.

Fig 2 Aggregated per 0.5° cell results of global distribution, latitudinal patterns (note the different scales per panel of SOC stocks change), and continental bar plots of changes of soil organic carbon (SOC) stocks from 2009 to 2020 (0 ~ 100 cm soil depth) in mangroves, salt marshes and tidal flats. The bar graph shows the change of SOC stocks (10 Tg), SOC density (Mg/ha) and wetland area (10^3 km^2) of each continent. Note: AF: Africa; AS: Asia; OA: Australia and Oceania; EU: Europe; NA: North America; SA: South America. The change curves are calculated based on the mean SOC stock estimates. The spatial distribution of SOC stocks (0 ~ 100 cm) for mangroves, salt marshes, and tidal flats in 2009-2014 and 2015-2020 are shown in Fig S2A and Fig S2B. Fig S3 shows the latitudinal patterns of SOC stocks (2009-2014 and 2015-2020) and their changes across soil depths (0 ~ 30 cm, 30 ~ 60 cm, and 60 ~ 100 cm) for mangroves, salt marshes, and tidal flats.

Fig 3 Differences in soil organic carbon (SOC) stocks changes (Tg) in different income level countries from 2009-2014 to 2015-2020 (0 ~ 100 cm soil depth, signed log10) (A) and top SOC stocks losses (10) and gains (4) by country between 2009-2014 and 2015-2020 (0 ~ 100 cm soil depth) (B). L: low-income countries; LM: lower-middle income countries; UM: upper-middle income countries; H: high-income countries. Box hinges represent the upper and lower quartiles, with the horizontal line indicating the median. The whiskers extend to the most extreme data points within 1.5 times the interquartile range (IQR) from the upper and lower quartiles; "*" and "****" indicate significant differences in the SOC stocks change between the two groups at the 0.05 and

0.0001 significance level, respectively.

Fig 4 SHapley Additive exPlanations (SHAP)-based analysis of driving factors for soil organic carbon (SOC) across mangroves (A), salt marshes (B) and tidal flats (C). Note: Prec_mean, Tmax_mean, Tmin_mean: annual average of precipitation (Prec) and maximum temperature (Tmax), minimum temperature (Tmin); Prec_mean_1, Tmax_mean_1, Tmin_mean_1 (i.e., 1, 2, 3, 4): seasonal average of Prec, Tmax and Tmin, the four seasons are defined as March to May, June to August, September to November, and December to February, respectively. Other detailed covariate explanations can be found in Table S2.

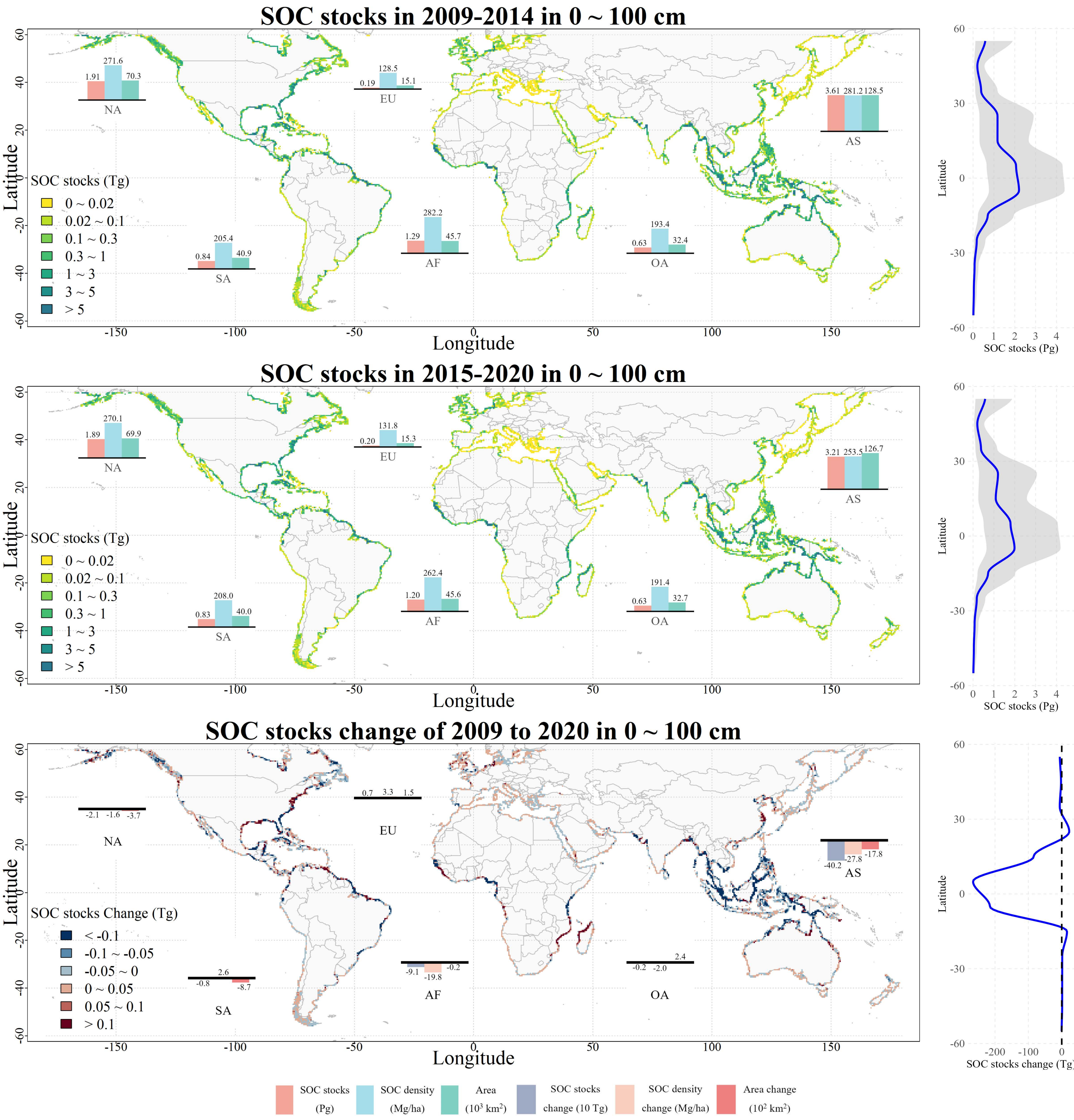
SOC stocks in 2009-2014 in 0 ~ 100 cm
SOC stocks (Tg)
0 ~ 0.02
0.02 ~ 0.1
0.1 ~ 0.3
0.3 ~ 1
1 ~ 3
3 ~ 5
> 5
NA 1.91 271.6 70.3
EU 0.19 128.5 15.1
AS 3.61 281.2 128.5
SA 0.84 205.4 40.9
AF 1.29 282.2 45.7
OA 0.63 193.4 32.4
Latitude
Longitude
SOC stocks (Pg)
SOC stocks in 2015-2020 in 0 ~ 100 cm
NA 1.89 270.1 69.9
EU 0.20 131.8 15.3
AS 3.21 253.5 126.7
SA 0.83 208.0 40.0
AF 1.20 262.4 45.6
OA 0.63 191.4 32.7
SOC stocks change of 2009 to 2020 in 0 ~ 100 cm
SOC stocks Change (Tg)
< -0.1
-0.1 ~ -0.05
-0.05 ~ 0
0 ~ 0.05
0.05 ~ 0.1
> 0.1
NA -2.1 -1.6 -3.7
EU 0.7 3.3 1.5
AS -40.2 -27.8 -17.8
SA -0.8 2.6 -8.7
AF -9.1 -19.8 -0.2
OA -0.2 -2.0 2.4
SOC stocks change (Tg)
SOC stocks (Pg)
SOC density (Mg/ha)
Area (10^3 km^2)
SOC stocks change (10 Tg)
SOC density change (Mg/ha)
Area change (10^2 km^2)

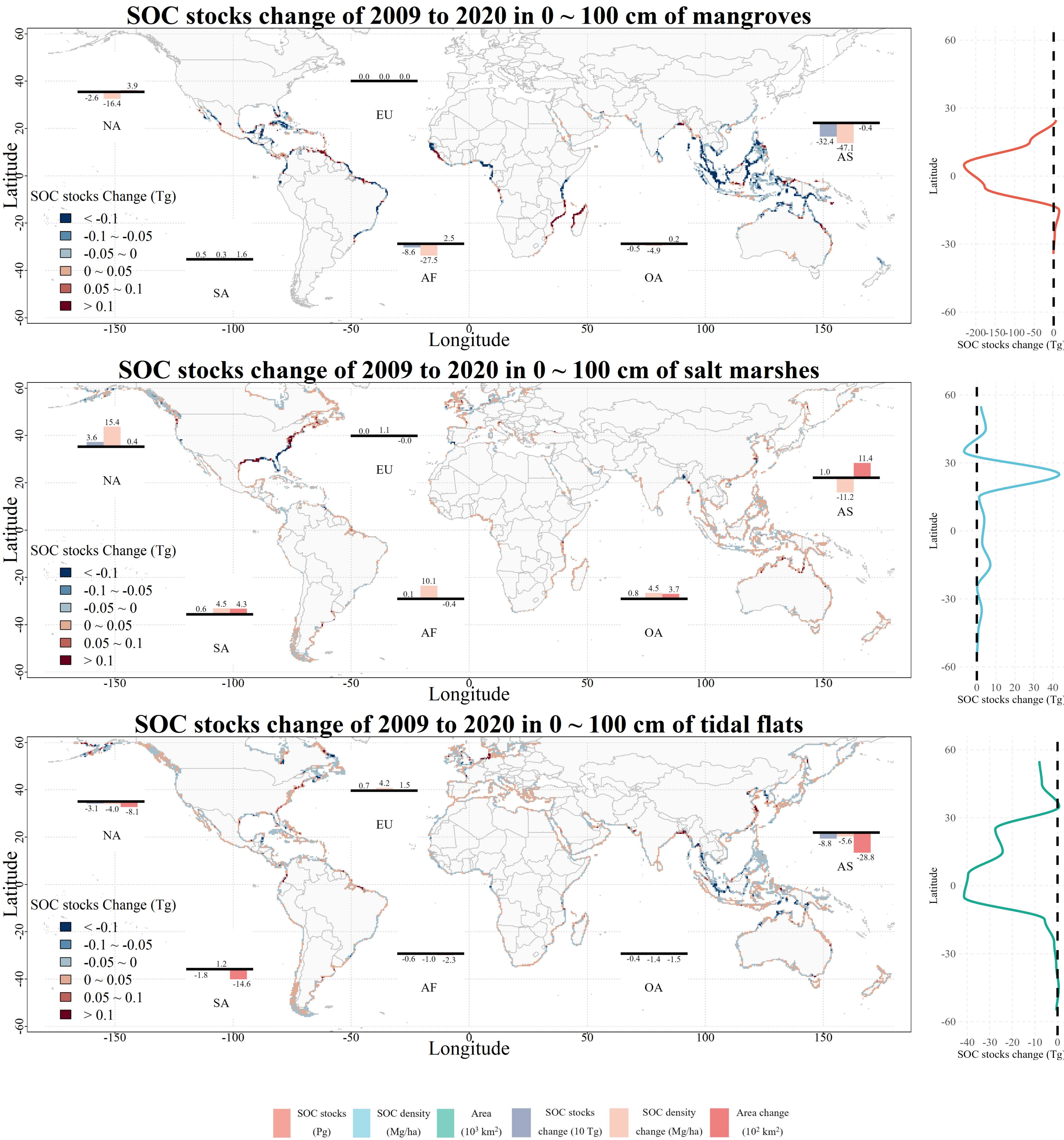
SOC stocks change of 2009 to 2020 in 0 ~ 100 cm of mangroves
SOC stocks change of 2009 to 2020 in 0 ~ 100 cm of salt marshes
SOC stocks change of 2009 to 2020 in 0 ~ 100 cm of tidal flats
Latitude
Longitude
SOC stocks Change (Tg)
< -0.1
-0.1 ~ -0.05
-0.05 ~ 0
0 ~ 0.05
0.05 ~ 0.1
> 0.1
NA
EU
AS
SA
AF
OA
SOC stocks change (Tg)
SOC stocks (Pg)
SOC density (Mg/ha)
Area (10^3 km^2)
SOC stocks change (10 Tg)
SOC density change (Mg/ha)
Area change (10^2 km^2)

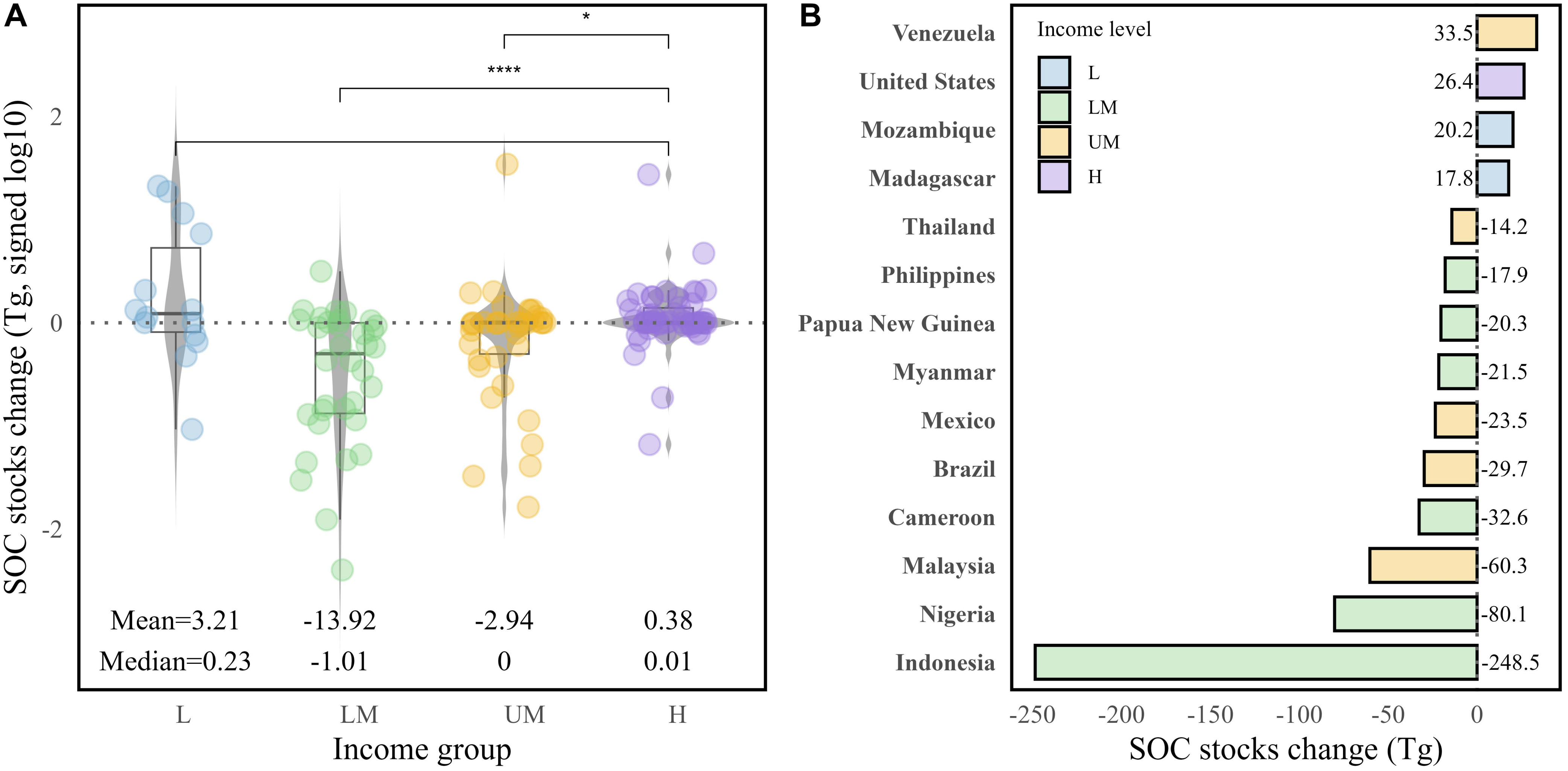
A
*
****
SOC stocks change (Tg, signed log10)
2
0
-2
Mean=3.21
-13.92
-2.94
0.38
Median=0.23
-1.01
0
0.01
L
LM
UM
H
Income group
B
Income level
L
LM
UM
H
Venezuela 33.5
United States 26.4
Mozambique 20.2
Madagascar 17.8
Thailand -14.2
Philippines -17.9
Papua New Guinea -20.3
Myanmar -21.5
Mexico -23.5
Brazil -29.7
Cameroon -32.6
Malaysia -60.3
Nigeria -80.1
Indonesia -248.5
-250
-200
-150
-100
-50
0
SOC stocks change (Tg)

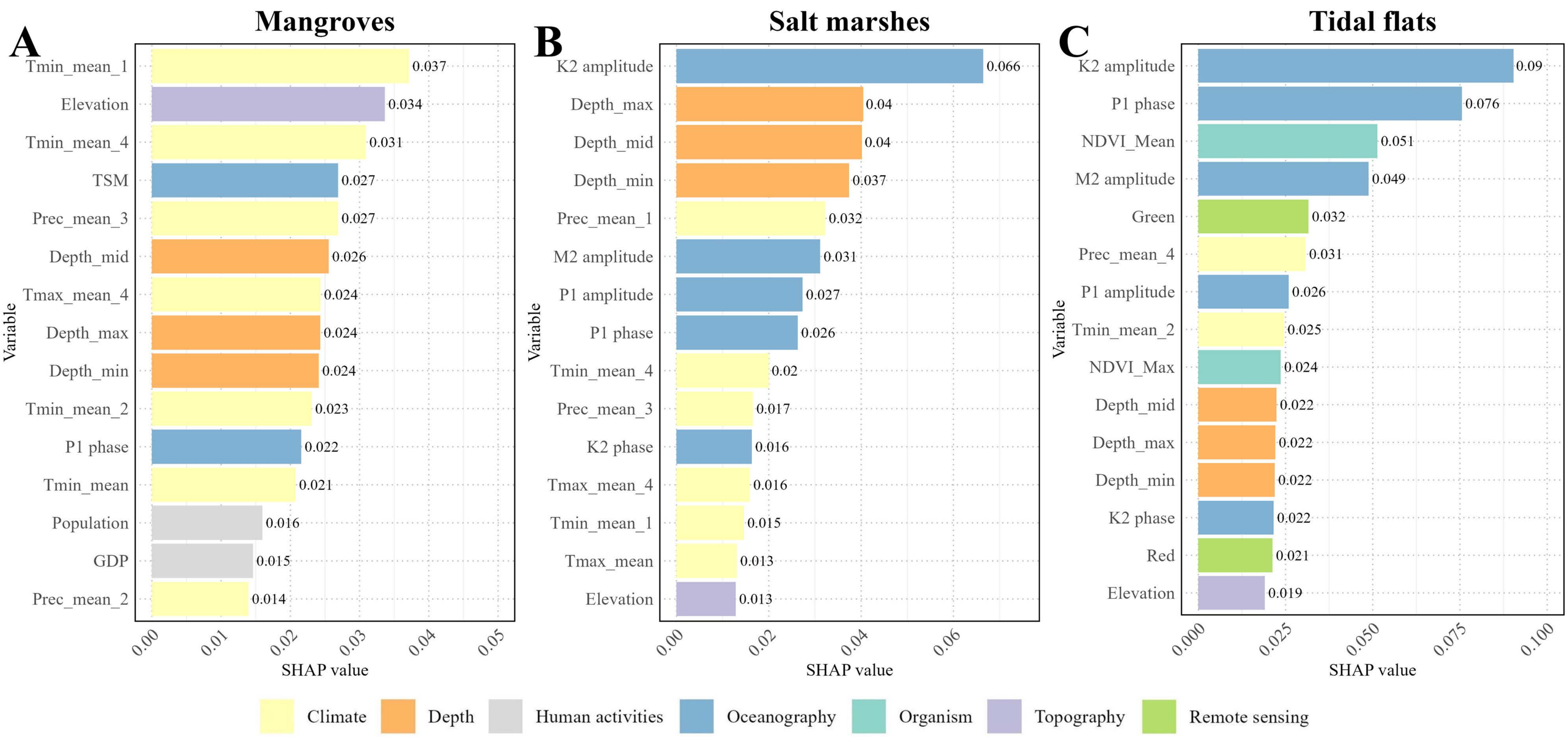
Mangroves
A
Tmin_mean_1 0.037
Elevation 0.034
Tmin_mean_4 0.031
TSM 0.027
Prec_mean_3 0.027
Depth_mid 0.026
Tmax_mean_4 0.024
Depth_max 0.024
Depth_min 0.024
Tmin_mean_2 0.023
P1 phase 0.022
Tmin_mean 0.021
Population 0.016
GDP 0.015
Prec_mean_2 0.014
Variable
0.00 0.01 0.02 0.03 0.04 0.05
SHAP value
Salt marshes
B
K2 amplitude 0.066
Depth_max 0.04
Depth_mid 0.04
Depth_min 0.037
Prec_mean_1 0.032
M2 amplitude 0.031
P1 amplitude 0.027
P1 phase 0.026
Tmin_mean_4 0.02
Prec_mean_3 0.017
K2 phase 0.016
Tmax_mean_4 0.016
Tmin_mean_1 0.015
Tmax_mean 0.013
Elevation 0.013
Variable
0.00 0.02 0.04 0.06
SHAP value
Tidal flats
C
K2 amplitude 0.09
P1 phase 0.076
NDVI_Mean 0.051
M2 amplitude 0.049
Green 0.032
Prec_mean_4 0.031
P1 amplitude 0.026
Tmin_mean_2 0.025
NDVI_Max 0.024
Depth_mid 0.022
Depth_max 0.022
Depth_min 0.022
K2 phase 0.022
Red 0.021
Elevation 0.019
Variable
0.000 0.025 0.050 0.075 0.100
SHAP value
Climate
Depth
Human activities
Oceanography
Organism
Topography
Remote sensing